NOAA Technical Memorandum EDS BOMAP-18

RADAR AND SATELLITE PRECIPITATION ANALYSIS OF A 5-DAY BOMEX DATA SAMPLE

Michael D. Hudlow

Washington, D.C.
December 1975

noaa NATIONAL OCEANIC AND ATMOSPHERIC ADMINISTRATION / Environmental Data Service

NOAA TECHNICAL MEMORANDA

Environmental Data Service, BOMAP Series

The Barbados Oceanographic and Meteorological Experiment (BOMEX) was conducted in May, June, and July 1969. Following the field experiment, the Barbados Oceanographic and Meteorological Analysis Project (BOMAP) was established in the Research Laboratories (ESSA), now NOAA, to coordinate the reduction of the data collected; to analyze these data, particularly those pertaining to the Sea-Air Interaction Program (the BOMEX Core Experiment); and to provide a central contact point for information exchange and publication of BOMEX results.

The name of the BOMAP Office was subsequently changed to Center for Experiment Design and Data Analysis (CEDDA), which was transferred to NOAA's Environmental Data Service in 1972. BOMAP remains, however, one of CEDDA's responsibilities, and publication of NOAA Technical Memoranda will continue as a means for disseminating information resulting from analyses of BOMEX data conducted at CEDDA. ERLTM-BOMAP-1 was published in the series of ESSA Technical Memoranda, ESSA Research Laboratories. ERL BOMAP-2 through ERL BOMAP-9 were issued as part of the series of NOAA Technical Memoranda, Environmental Research Laboratories. Subsequent publications are part of the series of NOAA Technical Memoranda, Environmental Data Service.

Publications listed below are available from the National Technical Information Service, U.S. Department of Commerce, Sills Bldg., 5285 Port Royal Road, Springfield, Va. 22151. Price: Paper copy prices vary; $2.25 for microfiche. Order by accession number shown in parentheses at end of each entry.

ESSA Technical Memoranda

ERLTM-BOMAP 1 High-Level Cloud Photography Inventory, BOMEX Period IV, July 11-28, 1969. Vance A. Myers, September 1970, 66 p. (PB-194-661)

NOAA Technical Memoranda

ERL BOMAP-2 A Statistical Data Plan for BOMEX. Theodore W. Horner, December 1970, 105 p. (COM-71-00188)

ERL BOMAP-3 Mass, Momentum, and Energy Budget Equations for BOMAP Computations. Eugene M. Rasmusson, January 1971, 32 p. (COM-71-00195)

ERL BOMAP-4 High-Level Cloud Photography Inventory, BOMEX Period II, May 24-June 10, 1969. Vance A. Myers, March 1971, 86 p. (COM-71-00574)

ERL BOMAP-5 Preliminary Velocity Divergence Computations for BOMEX Volume Based on Aircraft Winds. Robert W. Reeves, April 1971, 21 p. (COM-71-00667)

ERL BOMAP-6 Ship's Influence on Surface and Rawinsonde Temperatures During BOMEX. Warren M. Wisner, June 1971, 44 p. (COM-71-00950)

ERL BOMAP-7 High-Level Cloud Photography Inventory, BOMEX Period I, May 3-15, 1969. Vance A. Myers, December 1971, 55 p. (COM-72-10196)

ERL BOMAP-8 BOMEX Flight Tracks Reconstructed From Near-Simultaneous High-Level Cloud Photography by Two Aircraft. Vance A. Myers and Martin Predoehl, December 1971, 13 p. (COM-72-10313)

ERL BOMAP-9 The BOMEX Sea-Air Interaction Program: Background and Results to Date. Joshua Z. Holland, March 1972, 34 p. (COM-72-10576)

EDS BOMAP-10 BOMEX Rainy Day Analysis. Lt. Garry W. Elliott, July 1973, 9 p. (COM-74-10466)

EDS BOMAP-11 Method for Obtaining Wet-Bulb Temperatures by Modifying the Psychrometric Formula. J. Sullivan and L. D. Sanders, June 1974, 8 p. (COM-74-11425)

EDS BOMAP-12 Profiles in the Lowest 300 Meters of the Marine Tropical Planetary Boundary Layer. C. F. Ropelewski, September 1974, 24 p. (COM-74-11779)

EDS BOMAP-13 Water-Vapor and Mass Divergence Computations Based on BOMEX Aircraft and Rawinsonde Data: A Comparison. Robert W. Reeves, December 1974. (COM-75-10268)

EDS BOMAP-14 Geostrophic Motion for the BOMEX Oceanic Volume. Victor E. Delnore, March 1975, 24 p. (COM-75-10646)

(Continued on inside back cover)

NOAA Technical Memorandum EDS BOMAP-18

RADAR AND SATELLITE PRECIPITATION ANALYSIS OF A 5-DAY BOMEX DATA SAMPLE

Michael D. Hudlow

Washington, D.C.
December 1975

UNITED STATES
DEPARTMENT OF COMMERCE
Rogers C. B. Morton, Secretary

NATIONAL OCEANIC AND
ATMOSPHERIC ADMINISTRATION
Robert M. White, Administrator

Environmental Data
Service
Thomas S. Austin, Director

CONTENTS

	Page
NOTATION	v
ABSTRACT	vi
1. INTRODUCTION	1
2. DATA COLLECTION	1
2.1 Surface-Based Radars and Digitization of Radar Data	3
2.2 Airborne Radars	3
2.3. Satellite Measurements	3
2.4 Rain-Gage Measurements	4
3. WEATHER SYSTEMS	4
4. ANALYTICAL PROCEDURES	10
4.1 Analysis of Shipboard Rain-Gage Data	10
4.2 Statistical Model of Precipitation Echoes	11
4.3 Calibrations of Surface-Based Radars and Analysis of Radar Data	13
4.3.1 Radar Equation and Drop-Size Distribution	13
4.3.2 Overall Calibration Derived From Comparison of Island Radar and Island Rain-Gage Data	14
4.3.3 Comparison Between the MPS-34 and METEOR-200 Radars	15
4.3.4 Attenuation Corrections	16
4.3.5 Empirical Adjustment for Non-Beam Filling	17
4.4 Analysis of Satellite Data	19
4.4.1 General Methodology	19
4.4.2 Relationship Between Diurnal Variation of Cloud Amount and Radar Echo Amount	20
4.5 Summary of Steps Taken in Deriving Rainfall Estimates From Radar and Satellite Data	22
5. DISCUSSION OF RESULTS	22
5.1 Rain-Gage Analysis	22
5.2 Space and Time Variations of Cloud and Echo Amount	25
5.3 Six-Hourly, Daily, and 5-Day "Best Estimates" of Rainfall Amounts	27
5.4 Comparison of Results With Previous Studies	28

CONTENTS (Continued)

Page

6. ASSESSMENT OF ERRORS 29

6.1 Error Expected Under Standard Operational Conditions 29
6.2 Sources of Error 30
6.3 Errors Characteristic of BOMEX 31

6.3.1 Overall Calibration Procedures 33
6.3.2 Sampling Errors 33
6.3.3 Attenuation by Liquid Water 34
6.3.4 Accuracy of the Statistical Echo Model 34
6.3.5 Adjustment for Bon-Beam Filling 35
6.3.6 Extrapolation With Satellite Data 38
6.3.7 Summary of Probable Confidence Limits 38

7. CONCLUDING REMARKS 42

ACKNOWLEDGMENTS 44

REFERENCES 44

NOTATION

A = any area for which a precipitation estimate is derived

A_i = fraction of the total area of the BOMEX square contained in subsection i

A_{ei} = the radar echo area persisting at a receiver gain threshold, i

b = slope coefficient in the exponential model that describes the spatial distribution of power returned from a radar precipitation echo; eq. (1)

C = radar constant

D = radar echo length (maximum dimension)

e_b = expected standard or base error factor

e_{ij} = maximum probable error factor due to source i and for j time interval

E = an estimate of precipitation

F = ratio of areal radar estimate for radar ranges of less than 100 mi to the areal radar estimate for radar ranges beyond 100 mi

m = complex index of refraction

n = number of observations in a sample used for error analysis

N = number of radar echoes within an area, A

p = percent error for a single estimate

$\bar{p}$ = average percent error for all estimates in a sample

$\bar{P}_r$ = average power returned to the radar receiver from a pulse volume containing precipitation particles

$\bar{P}_{ri}$ = threshold power returned to the radar receiver at gain setting, i

$\bar{P}_{rm}$ = intercept coefficient in the exponential model which describes the spatial distribution of power returned from a precipitation echo; eq. (1)

r = slant range to radar target

R = rainfall rate at a point

$\bar{R}$ = average rainfall over an area, A

T = true or actual amount of precipitation

Z_e = equivalent reflectivity factor

γ = attenuation coefficient

ρ = correlation coefficient

ABSTRACT

Radar and satellite data are used qualitatively and quantitatively to describe the precipitation morphology for a 5-day period of the Barbados Oceanographic and Meteorological Experiment (BOMEX), conducted in 1969. The period was characterized by undisturbed weather conditions, but was immediately preceded and followed by moderate and mild disturbances, respectively. Typical satellite and radar photographs are presented to illustrate cloud patterns and precipitation echoes. Minimums of cloud and echo amount are generally observed around midday; maximums, in the early morning hours. Average echo and cloud amounts for the period were found to decrease with increasing north latitude.

Procedures for calibrating and optimizing the use of the quantitative radar data are discussed. Average rainfall rates for areas of several thousand square miles and for intervals as short as 6 hr are estimated by means of a statistical echo model that relates rainfall rate to the lengths of observed radar echoes. For selected time periods, precipitation amounts are also derived directly from digitized "gain-step" data, and comparisons are made between this direct approach and the indirect statistical model method. Satellite cloud data are used to extrapolate the rainfall estimates to areas not covered by radar.

The best estimate for the average rate of rainfall deposited over the BOMEX square (96,000 mi^2) during the 5-day period was found to be about 0.35 mm/day, an estimate believed to be accurate within a factor of 2.5.

RADAR AND SATELLITE PRECIPITATION ANALYSIS OF A 5-DAY BOMEX DATA SAMPLE

Michael D. Hudlow
Center for Experiment Design and Data Analysis
Environmental Data Service
National Oceanic and Atmospheric Administration

1. INTRODUCTION

The "Core Experiment" of the Barbados Oceanographic and Meteorological Experiment (BOMEX) was designed for study of sea-air interactions through determination of heat, momentum, and water budgets. During the 1969 field operations, atmospheric sampling was concentrated within a 500-km x 500-mb "box" east of the island of Barbados. Ocean salinity and temperature were measured routinely down to 1,000 m.

For meaningful budget studies, a knowledge of the statistical character and quantity of clouds and precipitation within the experimental volume is required. During BOMEX, surface-based and airborne radars, shipboard rain gages, and infrared and visible sensors carried on satellites were the means by which data were obtained for evaluating the precipitation term in the budget equations. These equations have been formulated by Rasmusson (1971).

This report deals with the precipitation analysis and morphology for one subset of BOMEX data covering the 5-day period from June 22 through June 26, 1969. Six-hourly time increments were adopted as the basic interval for deriving areally averaged precipitation rates.

Various other aspects of the Core Experiment and results of continuing analyses of BOMEX data have been discussed by Holland (1970, 1972a and b) and by Holland and Rasmusson (1973). For an overall description of BOMEX, including sensors used and experiments carried out by individual investigators, the reader is referred to BOMEX Field Observations and Basic Data Inventory (BOMAP Office, 1971).

2. DATA COLLECTION

Land-based, shipboard, and airborne radar observations were used to record precipitation echoes. Location of the two surface-based radars and the flight track for the aircraft radar photography are shown in figure 1.

Both visible and infrared satellite data augment the radar coverage. Satellite cloud photographs provide information on the temporal and spatial distribution of clouds, and from the infrared data minimum cloud-top temperatures can be mapped. Sources of supplementary data were rain gages mounted on each of the five BOMEX fixed ships--four stationed at the corners of the BOMEX square and one in the center--and a rain-gage network on Barbados.

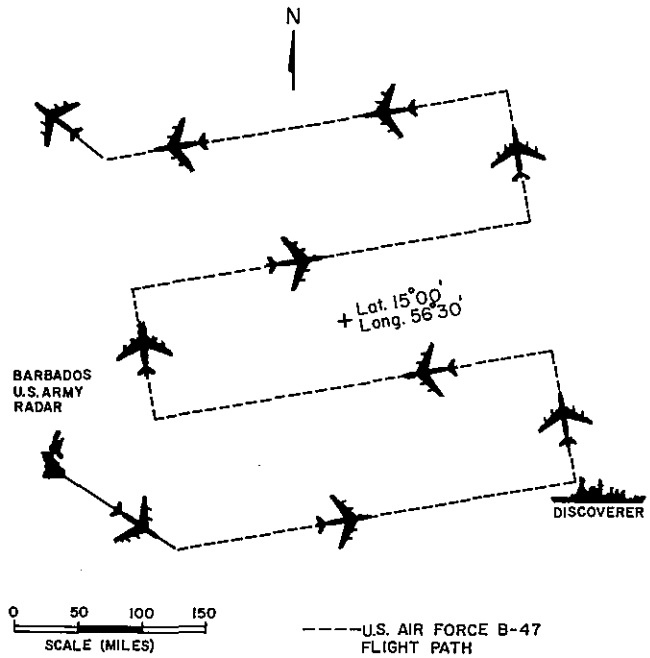

Figure 1.--Locations of surface-based radars and radar aircraft flight track used during BOMEX.

Table 1.--Characteristics of the MPS-34 and METEOR-200 radars (long pulse)

Characteristics	Nominal value	
	MPS-34	METEOR-200
Transmitted power (peak)	180 kW	175 kW
Wavelength	3.2 cm	3.2 cm
Antenna shape	Parabolic	Parabolic
Horizontal and vertical beam widths	1°	1.25°
Minimum detectable signal	-105 dBm	-97 dBm
Pulse repetition frequency	180 pps	240 pps
Pulse width	5×10^{-6} s	3×10^{-6} s

2.1 Surface-Based Radars and Digitization of Radar Data

The primary quantitative data for the southern half of the BOMEX box were obtained with a U.S. Army MPS-34 radar stationed on the island of Barbados and a NOAA METEOR-200 radar aboard the Discoverer, located at the southeastern corner of the BOMEX square. Characteristics of these two X-band radars are listed in table 1.

The METEOR-200 basic equipment is similar to the MPS-34 radar, which is described in detail in an earlier publication by this author (Hudlow, 1970a). The antenna and pedestal unit for the METEOR-200 was mounted on a gyro-stabilized platform that compensated for ship motion up to $\pm 25^{\circ}$ of roll and $\pm 10^{\circ}$ of pitch. The scope presentations were maintained relative to true north, regardless of ship's heading, through synchronization with the ship's gyrocompass. "Gain-stepping" of the radar receiver and scope photography were used in recording storm intensities with both radar sets.

For quantitative analyses by computer, many of the radar photographs collected for BOMEX have been digitized with a coordinate digitizer. Additional information on the digitizing and examples of computer printouts of digital displays from radar photographs taken during BOMEX are given in "BOMEX Permanent Archive: Description of Data" (Center for Experiment Design and Data Analysis, 1975).

2.2 Airborne Radars

A U.S. Air Force WB-47 aircraft equipped with an APS-64 radar collected radar photographs once daily along the flight path shown in figure 1 at an altitude of about 30,000 ft. The APS-64 is an X-band system with a dish providing 3.5° horizontal and 5° vertical beam widths. Mosaics of radar photographs obtained with this radar during several days of BOMEX--including the 5-day period analyzed in this report--have been prepared as a qualitative means for identifying precipitation areas. Examples of this type of presentation are given in BOMEX Period III Radar-Satellite Atlas (Scherer and Hudlow, 1975). NOAA's Research Flight Facility aircraft radar films were scanned on a microfilm viewer as an additional aid in obtaining background information on general weather conditions during the period under study.

2.3 Satellite Measurements

Infrared data from the Nimbus-3 satellite and visible data from the Applications Technology Satellite-3 (ATS-3) provided valuable supplementary inputs to complete the areal coverage of the BOMEX square.

Nimbus-3 high-resolution infrared (HRIR) data were obtained once a day at approximately local midnight; medium-resolution infrared (MRIR) data, twice daily, around local midnight and near local noon. These data consist of digital values of equivalent blackbody temperatures, presented in a mercator projection and gridded automatically by computer. Based on these data, fields of equivalent blackbody temperatures were analyzed, and isotherm maps were drawn for the 5-day period under study. A mean sounding, derived from

rawinsonde flights from all five BOMEX ships during the 5 days, was used to convert temperatures to heights for construction of isopleths of estimated minimum cloud heights from the HRIR isotherms. In the case of the MRIR data this was not done; the isotherms were used for direct identification of cloud distributions. The ground resolutions at a subsatellite point for the HRIR and MRIR scanning radiometers are 5.3 and 35 mi, respectively, according to the Nimbus III User's Guide (Sabatini, Ed.).

Three gridded and enlarged ATS-3 photographs were available for each day--one shortly after sunup, one around midday, and one close to sundown. Gridding was done by manually fitting a transparency containing geographical coordinates and land features to the satellite hemispherical disk. ATS-3 photographs lend themselves to this gridding procedure because they contain the horizon and normally reveal prominent coastal features. Also, it is possible in many instances to check the validity of the gridding of these photographs by comparing the location of the visible cloud areas with the position of precipitation echoes revealed by radar. The ATS-3 data used in this analysis were collected with the geostationary satellite located above a subsatellite point near the BOMEX area. The spatial resolution at the subsatellite point is 2.5 mi.

The gridding accuracy of both the visible and infrared satellite data used in this study is believed to lie within about 30 mi.

2.4 Rain-Gage Measurements

A rain gage was mounted on a boom extending from the bow of each of the five BOMEX fixed ships. Consisting of a collector 3 in. in diameter and an attached hose for depositing the collected precipitation into a clear cylinder graduated to the nearest 1/100 of an inch, the gage was mounted, nongimbaled, at deck level about 20 ft from the tip of the bow. Cumulative precipitation amounts to the nearest 1 mm were manually recorded and transcribed onto surface observation forms every 1.5 hr, and other logs maintained by the ships' crews, e.g., the radar "bench" log and the general event log, provide additional information on rainfall occurrences. Precipitation was also measured by a rain-gage network in the extreme southeast part of Barbados.

3. WEATHER SYSTEMS

A part of the sequence of radar and visible and infrared satellite pictures for synoptic times published in BOMEX Period III Radar-Satellite Atlas (Scherer and Hudlow, 1975) is presented in this section to illustrate the general weather conditions during the 5-day period of interest here. Visible satellite photographs for all four BOMEX Observation Periods (May 3 through July 28, 1969) are contained in BOMEX Atlas of Satellite Cloud Photographs (Myers, 1971).

The 5 days from June 22 through June 26 were free of significant convective disturbances. This undisturbed period was bracketed, however, by two convective disturbances--a moderate one that moved out of the BOMEX box

late on June 21 and a mild one that moved in late on June 26 and early June 27. This 5-day interval between disturbances is slightly greater than the mean interval of approximately 3.5 days obtained from data given by Frank (1970), who identified and categorized the Atlantic tropical systems for 1969 according to criteria linked with synoptic-scale perturbations in the wind and pressure fields. Since conventional radiosonde data and surface observations are scarce for ocean areas, satellite photographs are of particular importance in identifying such perturbations. Frank considers two broad categories of disturbances depending on the main source of energy: (1) those drawing primarily on latent heat and (2) those feeding mainly on a baroclinic source of energy. For example, the first category includes the Intertropical Convergence Zone and tropical waves, while the second includes upper cold lows. Based on this classification, the disturbances on both June 21 and June 27 were tropical waves originating over the African continent. The wave on June 21 produced wind shifts at San Andres, but the wave that passed Barbados on June 27 weakened and dissipated in the Caribbean (Frank, 1970).

Figure 2 is a composite of surface-based radar photographs taken at 1039 local time (l.t.) on June 21. It shows an extensive area of convective activity concentrated in the western part of the BOMEX box. Nimbus-3 MRIR data recorded about 15 min later, at approximately 1056 l.t., was used in deriving the contoured map of equivalent blackbody temperatures shown in figure 3. To a first approximation, since temperature generally decreases with altitude, the colder the temperature, the higher the clouds.

Comparison of figures 2 and 3 reveals good spatial correlation between areas contained within the cold isotherms and the radar echoes observed with the radar on Barbados. Since the absolute gridding of the MRIR products is accurate to within only about 30 mi, however, the spatial "fix" of the contours in figure 3 might be in error by that magnitude.

Figure 3 shows a region of cold temperatures (high cloud tops) over the northwest part of the BOMEX box beyond the ranges of the surface-based radars. From examination of all radar and satellite data for June 21 and from analysis of radar and satellite observations for other days during BOMEX, it is concluded that significant convective activity also was present in this region of cold temperatures.

A composite of radar photographs for 2225 l.t. on June 21 is shown in figure 4, which illustrates that convection becomes quiescent by the beginning of the 5-day period under study.

Figure 5 and 6 typify the radar echo and satellite cloud patterns prevalent during the 5 days. Of importance is that most of the cloud cover in the satellite photograph (fig. 6) over the BOMEX square is unaccompanied by precipitation echoes as revealed by the radar photographs (fig. 5), and that this cloud cover lies predominantly over the southern half of the BOMEX square.

The echo and cloud patterns in the radar and satellite photographs taken around 1625 l.t. on June 26 (figs. 7 and 8), show the mild disturbance that entered the east side of the BOMEX square toward the end of the 5-day period.

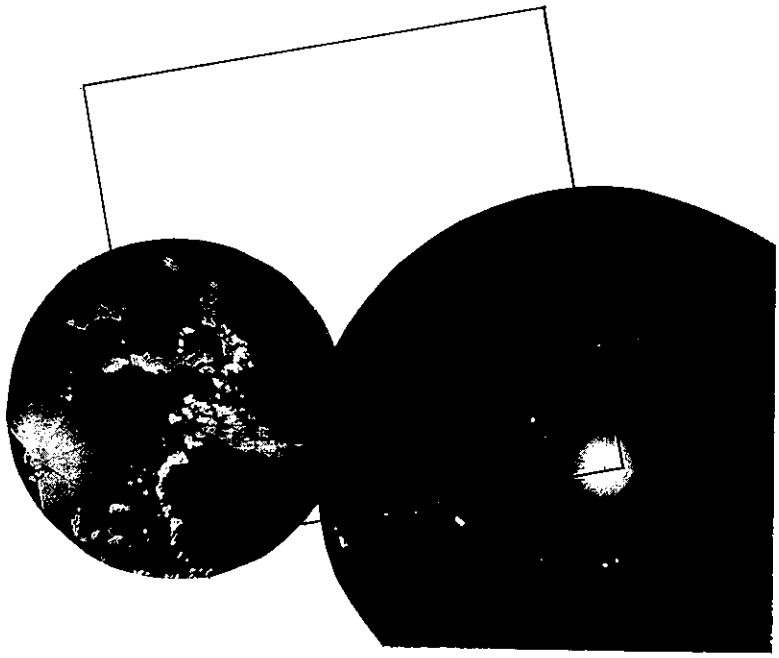

Figure 2.--Composite of surface-based radar photographs for June 21, 1969, 1039 l.t., with BOMEX square illustrated.

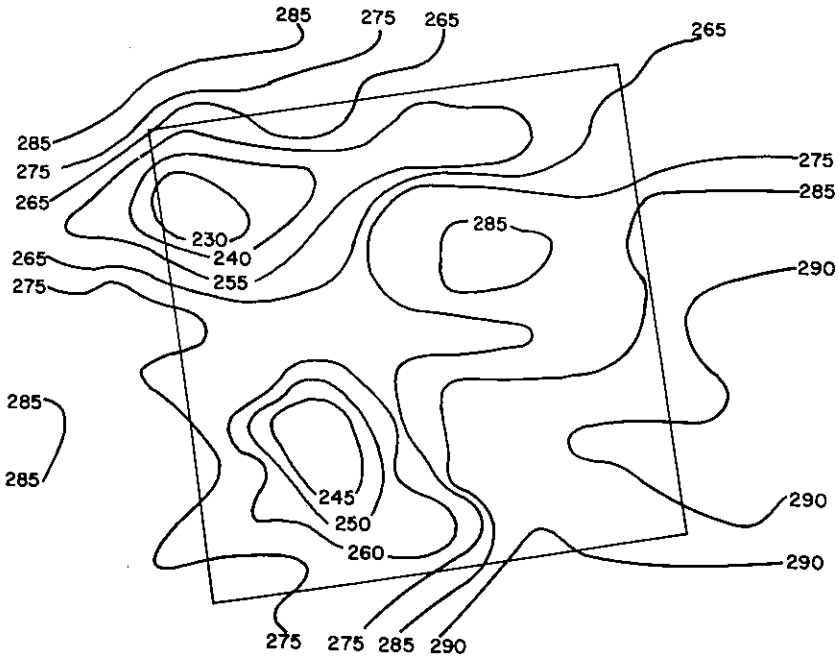

Figure 3.--Contoured map of equivalent blackbody temperatures (Kelvin) derived from Nimbus-3 MRIR data for June 21, 1969, 1056 l.t., with BOMEX square illustrated.

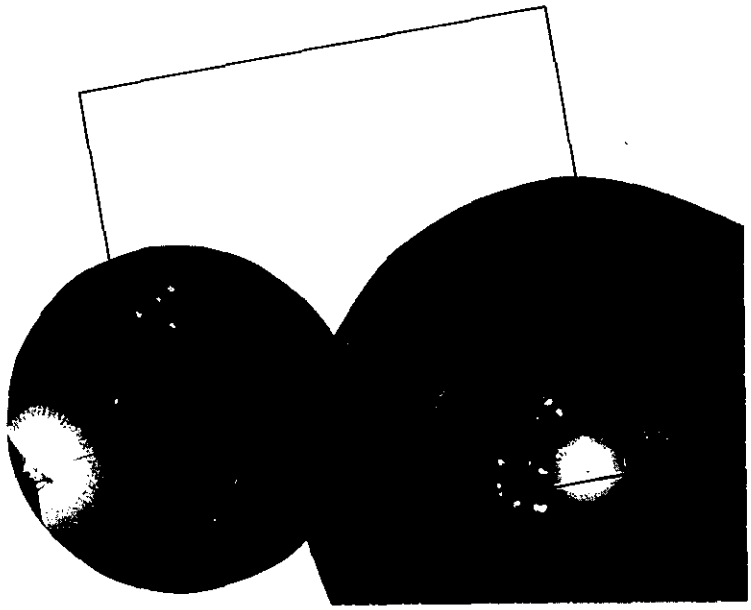

Figure 4.--Composite of surface-based radar photographs for June 21, 1969, 2225 l.t., with BOMEX square illustrated.

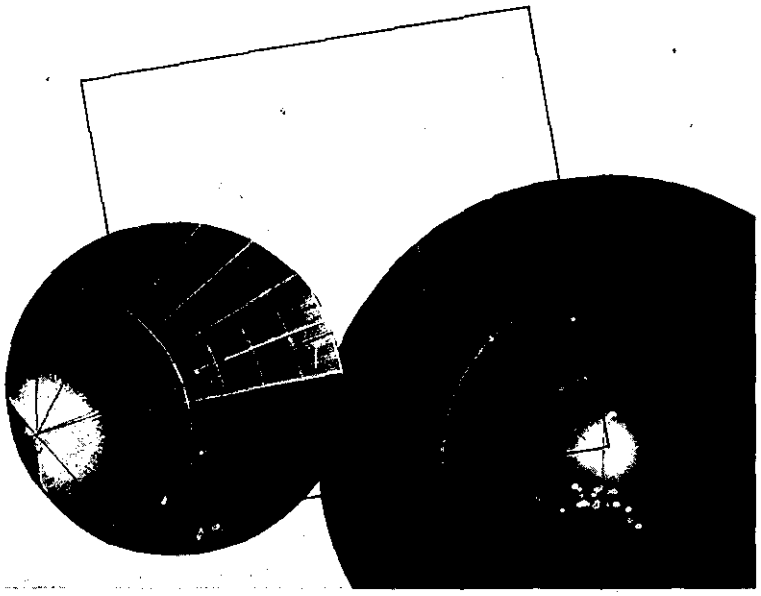

Figure 5.--Composite of surface-based radar photographs for June 23, 1969, 1630 l.t., with BOMEX square illustrated.

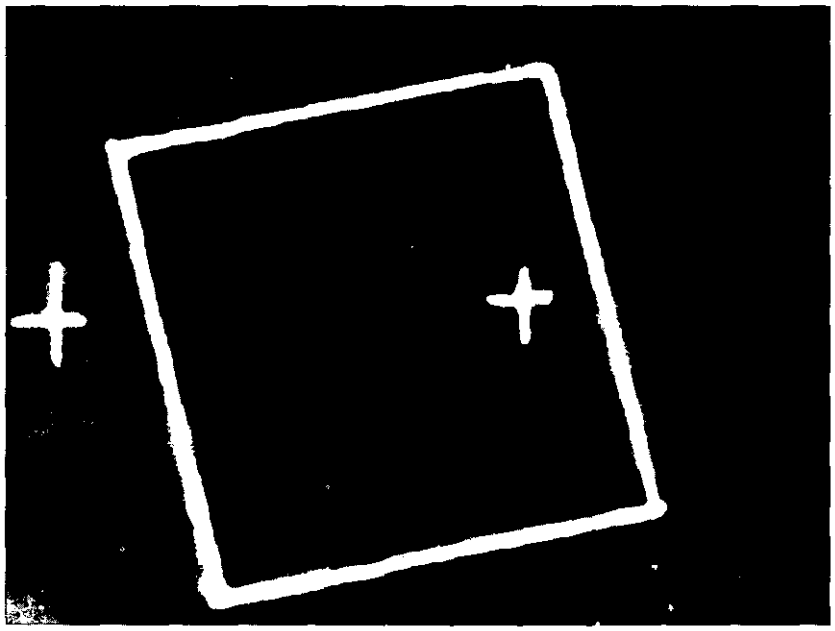

Figure 6.--Enlargement of ATS-3 photograph for June 23, 1969, 1630 l.t., with BOMEX square illustrated.

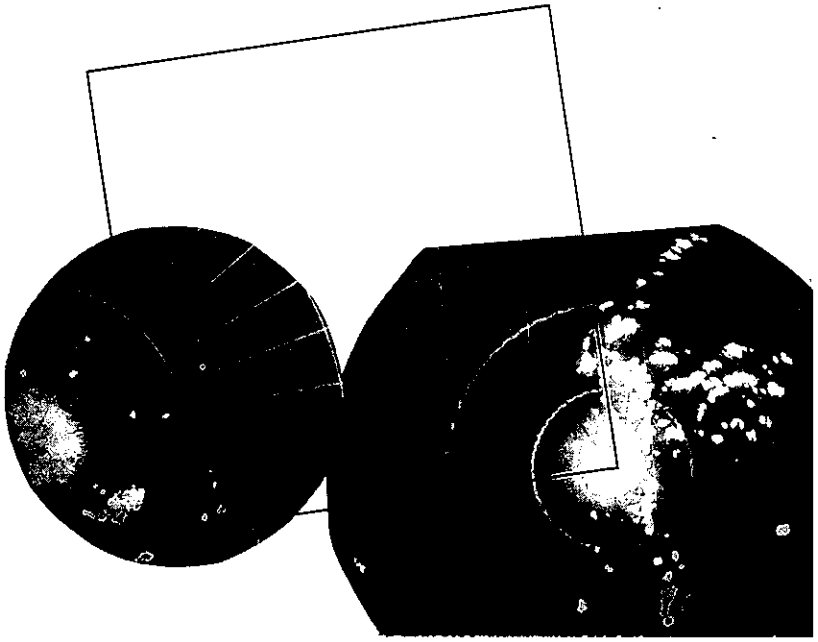

Figure 7.--Composite of surface-based radar photographs for June 26, 1969, 1614 l.t., with BOMEX square illustrated.

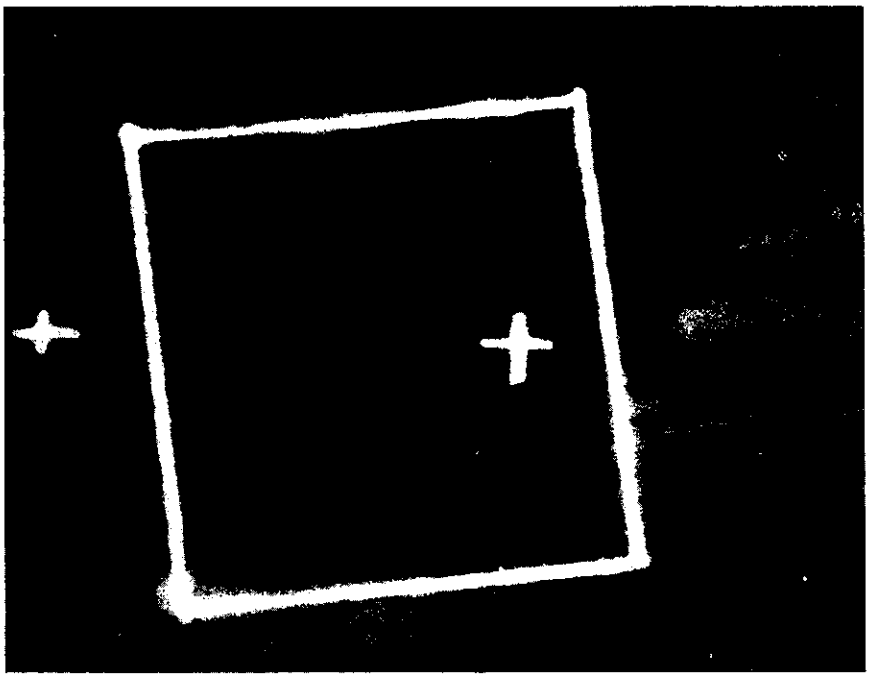

Figure 8.--Enlargement of ATS-3 photograph for June 26, 1969, 1635 l.t., with BOMEX square illustrated.

4. ANALYTICAL PROCEDURES

The quantitative data collected with the two surface-based radars are the primary ones for deriving rainfall estimates. Since radar can monitor and record precipitation occurrences almost continuously in time and space at ranges up to 200 mi, it is superior to a sparse rain-gage network. At best, a rain gage provides a true measure only at one point in space, and precipitation, especially in tropical regimes, can vary appreciably over short distances. Consequently, the BOMEX ship rain-gage network, with a density of one gage per 20,000 mi^2 is useful only as a relative consistency check for the radar analysis.

The surface-based radar data in their raw form are limited in several respects. One limitation stems from the fact that they cover only the southern half of the BOMEX box (fig. 1). Another arises from degradation due to non-beam filling, which becomes serious for the radar data collected beyond ranges of 100 mi. Still another limitation results from attenuation uncertainties accompanying X-band wavelengths. Finally, certain supplementary data, e.g., drop-size data, which are helpful for absolute calibration of the radar data, were not collected as an integral part of BOMEX.

To extend the usefulness of the radar data and to partly compensate for the limitations inherent in them, corrections and refinements were introduced. The scope and success of these refinements, and the overall approach for deriving quantitative precipitation estimates, are presented in the sections that follow.

4.1 Analysis of Shipboard Rain-Gage Data

As summarized by a working group of the Commission for Maritime Meteorology (World Meteorological Organization, 1962): "The ideal gauge for use on shipboard has not yet been found." This same report discusses the many difficulties associated with rain-gage measurements at sea. The obvious conclusion to be drawn from the WMO report is that to obtain reliable quantitative measurements from conventional rain gages requires good gage exposure, and laborious corrections for pitch and roll of the ship may be necessary. Even with optimum exposure of the rain gage, errors due to sea spray and turbulence may be significant during conditions of high winds and seas.

The rain-gage data obtained on board the five ships were used in their raw tabulated form, except in instances where obvious observer errors were spotted by cross-checking against the event and radar "bench" logs. Arithmetic averages for the BOMEX box were computed from the five-station network. Because of the low gage density represented by this network and because the accuracy of shipboard rain-gage measurements are in general inferior to measurements on land, the radar and satellite data remain the principal sources for deriving quantitative precipitation estimates.

4.2 Statistical Model of Precipitation Echoes

A quantitative statistical model that describes the vertical extent, the horizontal intensity distribution, and the areal coverage of a radar echo (given a one-dimensional parameter of the echo to serve as the independent variable) has been developed from BOMEX radar data (Hudlow, 1971). A description of the analytical techniques used in deriving the radar parameters for the model are given by Hudlow and Scherer (1975). The scope here is confined to a summary of concepts and to the uses, advantages, and limitations of the model. Results from other investigators are reviewed to provide perspective on the generality of the analytical expression that describes the areal intensity distribution within an echo.

The model has the following advantages:

(1) It can be used for deriving quantitative precipitation estimates from echo geometric measurements at ranges exceeding 100 mi from the radar, ranges for which meaningful gain-step measurements are unlikely (Hudlow, 1970a). (Only 12 percent of the BOMEX experimental area was covered by ranges less than 100 mi from the radar.)

(2) It can be used for deriving quantitative estimates when only maximum gain data (no gain-stepping) are available.

An expression relating the spatial distribution of radar power returned from an echo to the length of the echo was formulated after a detailed analysis of radar intensity (gain-step) data for 60 radar echoes, ranging in length from 4 to 150 mi. An exponential model was derived that relates threshold received power, $\overline{P}_{ri}$, to the square root of the echo area, $\sqrt{A_{ei}}$, persisting at a gain threshold, i:

$$\overline{P}_{ri} = \overline{P}_{rm}\, 10^{-b\sqrt{A_{ei}}} \quad . \tag{1}$$

The intercept, $\overline{P}_{rm}$, and slope, b, coefficients were found to correlate to a significant degree with the echo length (correlation coefficients: $\rho_{\overline{P}} = 0.71$, $\rho_b = 0.94$). $\overline{P}_{rm}$ represents the maximum power returned to the radar from the intensity peak within an echo. From the radar equation and an assumed raindrop-size model (sec. 4.3.1), eq. (1) can be transformed to yield a similar expression for rainfall rate (mm/hr) and/or precipitation content (g/m^3). The depth-area expression for rainfall resulting from this transformation, when integrated over a horizontal slice through a radar echo, gives an estimate of the total precipitation content at a certain altitude. Integration for several echo sizes has revealed that an estimate for the average rainfall rate at the surface, $\overline{R}$, based on a number of echoes within an area of interest, A, is proportional to the sum of the echo lengths raised to the 2.75 power:

$$\overline{R} = \phi \left(\sum_{j=1}^{N} D_j^{2.75} \right) / A \quad , \tag{2}$$

where D is the maximum horizontal dimension (length) of a radar echo, N equals the number of echoes within the area, A, and ϕ indicates functional dependency, which is given by Hudlow and Scherer (1975). Equation (2) is for an instant in time, and the effect of echo duration as a function of echo size is not considered. The 2.75 exponent is reasonably close to what one would expect, for example, for hemispherical or cylindrical echoes with homogeneous liquid-water concentrations and mean vertical velocities that are linearly proportional to the heights of the echo summits.

The form of eq. (1) is similar to that given by several other investigators. Holtz (1968) describes a radar echo model for severe summer thunderstorms observed in the vicinity of Montreal. His model formulation can be transformed into an expression similar to eq. (1), except that $\sqrt[3]{A_{ei}}$ appears instead of $\sqrt{A_{ei}}$, and b is held constant. BOMEX analyses indicate that for small echoes (5 to 15 mi long) a simple exponential model is preferable; for echoes of intermediate size (15 to 45 mi long) a logarithmic, square root is best; and for large echoes (>45 mi long) a logarithmic, cube root is optimum. This implies that, on the average, larger gradients of liquid-water content exist in the larger storms. In adopting eq. (1), we assume that a logarithmic, square-root model can be applied for all echo sizes by allowing $\overline{P}_{rm}$ and b to vary as a function of echo size. Altman (1970), using radar data from the National Severe Storms Laboratory (NSSL), has found logarithmic, square-root profiles to exist in many Oklahoma thunderstorms.

From recording rain-gage data for a 400-mi^2 network containing 49 uniformly distributed gages, Huff (1968) analyzed depth-area relationships for heavy rain storms in central Illinois. His conclusion, that a logarithmic square-root relationship frequently accompanies Illinois storms of short duration, supports the decision to use the logarithmic square-root model for describing instantaneous distributions in the BOMEX analysis. Huff's results, which are based on independent data from rain gages, adds credence to the use of eq. (1) with radar data.

While the functional form of eq. (1) can be shown to hold for a wide variety of convective conditions, the intercept, $\overline{P}_{rm}$, and slope, b, coefficients will not only vary as a function of echo length but may vary for a given echo with the stage of development, the synoptic conditions, the geographic location, and radar characteristics.

Although the relationship between rainfall rate and echo length was derived from a nonstratified statistical analysis (the echoes were not stratified, for example, by origin or stage of development), eq. (2) should prove useful for purposes of this study, so long as there is sufficient integration in time, and the area, A, is relatively large. The basic computational period used here is 6 hr, and A pertains to the portions of the area within the BOMEX square covered by radar measurements.

Since only a small portion of the BOMEX square (12 percent) was covered by radar measurements at ranges of less than 100 mi, the radar rainfall estimates presented in section 5 were derived by use of eq. (2). For selected time periods and for radar ranges of less than 100 mi, rainfall estimates

derived from the statistical model are compared with rainfall estimates derived driectly from the gain-step data. The probable maximum error accompanying the use of the statistical model is estimated in section 6.3.4.

4.3 Calibrations of Surface-Based Radars and Analysis of Radar Data

The approach adopted here for deriving rainfall estimates from radar intensity measurements is the conventional one of solving the radar equation and an equation relating the rainfall rate to the equivalent reflectivity factor.

The following steps were taken for hardware calibration and overall calibration and analysis:

(1) Conventional hardware and film calibrations were performed daily in the field.

(2) A drop-size distribution, based on drop-size data observed at a location with a climatology similar to that of Barbados, was adopted.

(3) Rainfall estimates derived from measurements made with the island radar were compared with those obtained from a rain-gage network covering a 35-mi^2 area on Barbados.

(4) For a 1-hr test on June 18, 1969, while the Discoverer was berthed in Barbados, data collected with the island radar were compared with measurements made with the shipboard radar for areas of overlapping coverage.

(5) Corrections for attenuation due to oxygen, water vapor, and rainfall were derived.

(6) An empirical time-averaged adjustment factor for non-beam filling for ranges beyond 100 mi was derived.

The field calibrations for the island radar are documented in an earlier publication by this author (Hudlow, 1970a). Analogous field calibrations were performed for the shipboard system.

4.3.1 Radar Equation and Drop-Size Distribution

The average power, $\overline{P}_r$, returned to the radar receiver from a volume of precipitation particles filling a nonattenuated radar beam is given by

$$\overline{P}_r = \frac{C|K|^2 Z_e}{r^2} , \tag{3}$$

where C is a constant that depends on the radar equipment, and

$$K = \frac{(m^2 - 1)}{(m^2 + 2)} ,$$

where m is the complex index of refraction of the precipitation particles, Z_e is the target equivalent reflectivity factor, and r is the slant range to the target. The Probert-Jones (1962) formulation for C was adopted for this study.

Solving for Z_e from eq. (3) gives

$$Z_e = \frac{(r^2 \overline{P}_r)}{(C|K|^2)} . \tag{4}$$

Since $\overline{P}_r$ and r are explicitly given by radar measurements and C and $|K|^2$ are assumed constant for a particular radar, Z_e can be derived from eq. (4).

The magnitude of Z_e is related to the number and size of hydrometeors in the pulse volume. Also, the rainfall rate, R, is related to the drop-size distribution. A correlation between R and Z_e therefore exists, but each is affected differently by a change in the drop-size distribution, which in turn depends upon location, rain type, season, and other factors.

Empirical relationships relating rainfall rate to reflectivity have been derived from drop-size spectra collected at the earth's surface for several geographic locations (e.g., Mueller and Sims, 1969). Majuro in the Marshall Islands is climatologically similar to the areas in the vicinity of Barbados, and the Marshall Islands relationship given by Mueller and Sims was selected for the BOMEX analysis. The resulting R versus Z_e equation is

$$R = 0.018\ Z_e^{0.745} , \tag{5}$$

where R is the rainfall rate in mm/hr, and Z_e is the equivalent reflectivity factor in mm^6/m^3.

For time periods and areas covered by good BOMEX gain-step data, eqs. (4) and (5) can be used to obtain rainfall estimates. In addition, as described in section 4.2, eq. (2) was used for estimating rainfall over the southern half of the BOMEX square from a census of echo sizes.

4.3.2 Overall Calibration Derived From Comparison of Island Radar and Island Rain-Gage Data

Rainfall estimates derived from the MPS-34 radar data for several storms were compared with those obtained from a rain-gage network inside a 35-mi^2 area in the extreme southeast part of the island (fig. 9). The comparison showed the rainfall estimates based on the radar data to be lower than those obtained from the rain-gage analysis by an average factor of 4.7, which

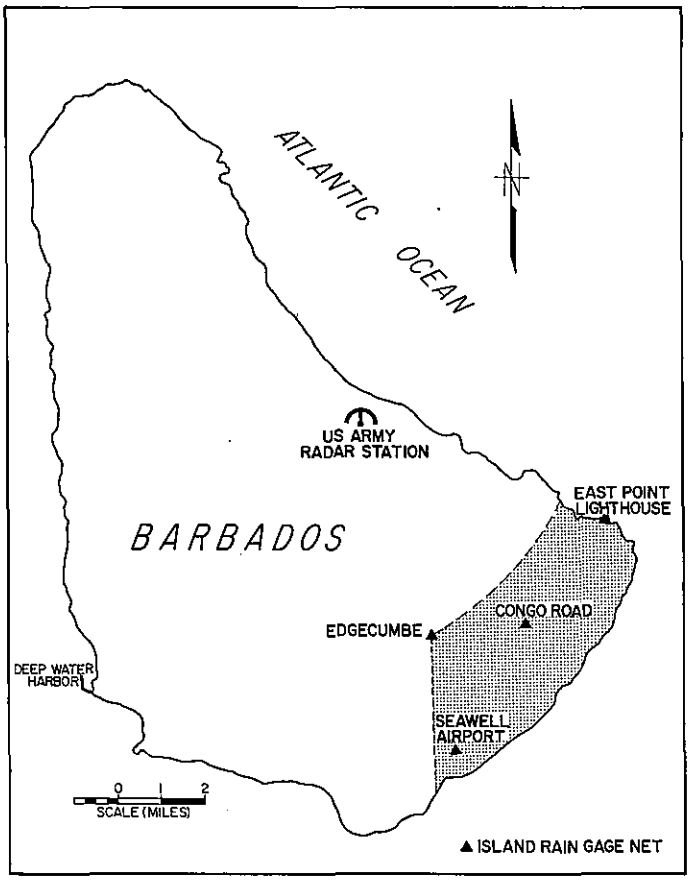

Figure 9.--Radar site and rain-gage network on the island of Barbados.

corresponds to a factor of about 8.0 (9 dB) in received power. Certain inaccuracies entering the solution of the radar equation often lead to underestimates, as have been reported by many investigators (Jones and Bigler, 1966). The exact reason for the MPS-34 underestimates is not known, but one likely source of error is an overestimate of the antenna gain (Hudlow and Scherer, 1975).

The radar gain-setting calibrations reported by this author (Hudlow, 1970a) were adjusted by 9 dB. The threshold values for the gain settings of the shipboard METEOR-200 radar were adjusted by the same magnitude. This was considered appropriate, since a comparison of data from the two radars for the same echoes revealed no significant differences in intensity measurements.

4.3.3 Comparison Between the MPS-34 and METEOR-200 Radars

On June 18, 1969, while the Discoverer was berthed in Deep Water Harbor, Barbados (fig. 9), continuous gain-step measurements were made with the MPS-34 and METEOR-200 radars for 1 hr. About one dozen echoes observed within 100 mi

of the radar sites were studied during this period. After normalization for differences in radar constants, target ranges, and system sensitivities, the intensity measurements made with the two radars were compared. The results showed no discrepancies greater than 2 dB, which is within the accuracy of the calibration equipment and procedures, and it was concluded that the measurements made by the two radars were in agreement.

4.3.4 Attenuation Corrections

X-band transmissions are subject to attenuation caused by precipitation and atmospheric gases between the radar site and the target. Attenuation resulting from rainfall is of greatest concern, since (1) the source is highly transient, and (2) such attenuation can become quite large. Also, for long path lengths in a tropical atmosphere, attenuation caused by oxygen and water vapor becomes significant.

Attenuation corrections for atmospheric gases can be made relatively easily, as their magnitude depends only on atmospheric pressure and relative humidity, and approximate data for these two parameters are generally available. Table 2 contains attenuation values for a mean tropical atmosphere that are assumed to be valid for use in correcting the BOMEX radar data.

Table 2.--Attenuation by oxygen and water vapor for X-band radiation emitted at 0° tilt angle and passing through a mean tropical atmosphere along various path lengths

One-way path to target (mi)	Total two-way attenuation caused by H_2O and O_2 (dB)
30	1.4
40	1.9
50	2.3
60	2.8
70	3.2
80	3.6
90	4.0
100	4.3

Amending eq. (4) to include an adjustment for attenuation resulting from rainfall yields

$$Z_e = \frac{\left(r^2 \, \overline{P}_r \, e^{2\int_0^r \gamma dr}\right)}{(C|K|^2)} , \tag{6}$$

where the exponential term is caused by liquid-water attenuation, γ is the attenuation coefficient (dB per unit distance), and r is the slant range.

Theoretically, given the distribution of the attenuation coefficient along the path, eq. (6) can be used to solve for Z_e. However, γ is a function of the drop-size distribution along the path, and since the drop sizes alter with time as well as location a unique distribution along the path cannot be determined. It is possible to empirically relate γ to Z_e or R. One such relationship, which is based on the drop-size distribution adopted for this study (sec. 4.3.1), is

$$\gamma = 0.12 \, R , \tag{7}$$

where γ is in dB/km and R is in mm/hr. Conceptually, one approach could consist of using eqs. (5), (6), and (7) to derive rainfall estimates, adjusted for liquid-water attenuation, by starting the solution at the radar site and proceeding outward; but, as pointed out by Hitschfeld and Bordan (1954), this approach can result in larger errors than will occur if no attempt is made to correct for attenuation. A primary difficulty is that the numerical coefficients in eq. (5), and to a somewhat lesser degree the one in eq. (7), are sensitive to changes in the drop-size distribution. Relatively small errors in these coefficients can result in significant errors in the estimates of R, especially at remote ranges, since the error accumulates with increasing range from the radar site as the integration of eq. (6) is performed.

In view of the above, the following procedure was adopted for processing BOMEX gain-step data:

(a) All initial estimates for R were derived by using eqs. (4) and (5), uncorrected for liquid-water attenuation.

(b) Attenuation adjustments were made to yield final R estimates, by first using eqs. (6) and (7), with the array of R's held fixed and equal to the first estimates, and then by solving for a new set of R's from eq. (5).

Although this procedure may not compensate sufficiently for the true effects of rainfall attenuation, it should not result in unrealistically large corrections, which can arise if the R's are adjusted as the integration in eq. (6) is performed and the estimate for each successively greater range is based on adjusted values up to that range.

4.3.5 Empirical Adjustment for Non-Beam Filling

Equation (3) is valid only when the radar beam is filled with precipitation particles. The likelihood of intercepting a representative

sample within the beam decreases as the distance to the target increases, because the radar beam widens and ascends above the surface of the earth as it travels away from the radar, until eventually even the tallest storms no longer fill the radar beam.

No satisfactory, explicit method exists for determining the degree of beam filling from individual radar measurements. It is possible, however, to derive statistics that give the average error caused by nonrepresentative beam sampling and non-beam filling--hereafter referred to as non-beam filling. This can be done by either (1) comparing radar with rain-gage data at various ranges or (2) assuming that for data covering a sufficiently long period all unexpected variations with range, observed in the averages for that period, are the result of deficient beam filling. Because suitable rain-gage data were unavailable, the second method was adopted for the analysis presented here. This decision might be questioned since the period under study consists of only 5 days. This brief period was, however, relatively free of convective disturbances, and the north-south variations were found approximately equal at all longitudes, indicating homogeneity in the east-west direction (Hudlow and Scherer, 1975). An important requirement implicit in the empirical procedure described below for deriving non-beam filling adjustments is the existence of east-west homogeneity in the average echo amount for the 5-day period.

As discussed by Hudlow (1970a), meaningful precipitation estimates are difficult to make by conventional procedures from gain-step measurements for ranges beyond about 100 mi. Quantitative estimates have been derived from BOMEX data for such ranges by means of the statistical echo model described in section 4.2 and by the following step-by-step procedure, which incorporates an adjustment for non-beam filling:

(1) Calculate for each surface-based radar, from eq. (2) and the census of echo lengths, the area-averaged rainfall rates for (a) areas inside the BOMEX box and within 100 mi of the radar site, and (b) areas inside the BOMEX box but at ranges beyond 100 mi.

(2) Compute within each radar umbrella the total precipitation deposited during the 5-day period over areas (a) and (b), based on the rainfall estimates derived above.

(3) Determine for each radar the ratio given by dividing the accumulated average precipitation for area (a) by the one for area (b) for the 5-day period.

(4) Adjust the rainfall estimates for individual time increments of 6 hr with these ratios under the assumption that they are applicable to each 6-hr period within the 5 days.

This approach for adjusting the radar data for non-beam filling at ranges beyond 100 mi has obvious shortcomings, but it does give improvement over the unadjusted data. For the 5-day period, the ratios between accumulated average precipitation for areas (a) and (b) were 5.5 for the island-based radar and 13.5 for the shipboard radar. The substantially larger ratio for the shipboard radar can partially be attributed to the combination of a larger beam width (1.25° compared with 1.0° for the island

radar) and a shorter radar horizon. The antenna for the shipboard radar was only about 65 ft above sea level, while the island radar was located 950 ft above mean sea level (Hudlow, 1970a). The shipboard radar also suffered beam losses from sea absorption and reflection, because it was operated normally at a base antenna-tilt angle of 0°.

The probable maximum error introduced into the precipitation estimates by the above procedure, including adjustments for non-beam filling, is discussed in section 6.

An empirical adjustment factor could be derived as a continuous function of range. The importance of doing this depends on the size of the area for which the precipitation estimate is being derived. Because of the small data sample used here, the adjustments were not graduated into smaller range increments. With additional digital data now available (CEDDA, 1975), it may be useful to determine the range dependency for finer range increments (25-mi increments being sufficient). If this is done, the data should be stratified into a minimum of two classes, one for disturbed and the other for undisturbed weather.

4.4 Analysis of Satellite Data

4.4.1 General Methodology

Since no quantitative radar data are available for the northern 50 percent of the BOMEX box, satellite data were used to extrapolate the rainfall estimates for the southern half to the northern half. The fundamental supposition is that the ratios obtained by dividing the average cloud amounts over the southern half of the BOMEX box, for each 6-hr interval, into those for the northern half are equal to ratios based on average rainfall for the same areas and times.

Cloud amounts were estimated from satellite data, and since these data are available for the entire BOMEX box, the north-south ratio derived from satellite cloud data provides a means of extrapolating rainfall estimates to the northern half of the box. If the cloud types over the entire BOMEX area were reasonably homogeneous, then the ratios used in the rainfall extrapolation procedure will be realistic. In any case, since cloud amounts in the northern part of the BOMEX box were significantly smaller than in the south, the extrapolation is in a stable direction.

Based on a comparison of HRIR and radar data for 14 cases during BOMEX (Scherer and Hudlow, 1971), it has been observed that unless cloud height isopleths derived from the HRIR data exist above 550 mb the weather is largely characterized as undisturbed, with relatively insignificant amounts of convection. Applying this criterion to the entire BOMEX box verifies that undisturbed conditions prevailed during the 5-day period at all times for which infrared data are available (sec. 2.3).

4.4.2 Relationship Between Diurnal Variation of Cloud Amount and Radar Echo Amount

The procedure for deriving a diurnal curve from radar data, showing the average amount of radar echo coverage over a specified area for various times during the day, consists of computing the average for each time based on the total number of days contained in the period under study. Such a curve for the 5-day period is presented in figure 17, section 5.2.

The derivation of a diurnal curve for cloud amount from satellite data is not as straightforward. Since the ATS-3 system provides data only during the daytime, Nimbus-3 infrared satellite data were used for nighttime coverage. Because the two satellites have different instrument response characteristics and sensitivities to various cloud types, some method of normalization must be applied before cloud amount data derived from these two sources can be related on the same numerical scale. The following procedure was used in obtaining a diurnal curve of average cloud amount for the 5-day period based on ATS-3 data:

(1) Average cloud coverages during the 5 days were calculated for morning, midday, and afternoon, corresponding to the times of the gridded and enlarged ATS-3 photographs (sec. 2.3).

(2) A straight-line curve was drawn by connecting the three ATS-3 data points, and this curve was compared with the diurnal daytime curve derived from radar echo amounts.

(3) The comparison showed a correspondence between the two daytime curves, and the curve based on the ATS-3 cloud amount data was then extrapolated to cover the nighttime hours, under the assumption that the same correspondence between cloud and echo amount holds true for the nighttime period.

The diurnal variation of average cloud amount derived by the above procedure is shown in figure 10. Although there are several uncertainties related to the derivation of this curve, such as geographical gridding inaccuracies and change in illumination and camera response with varying solar zenith angle, the correspondence with the radar data in this instance lends credence to the results.

From the nighttime Nimbus-3 data, the average areal coverage subtended by the 800-mb isopleth corresponding to cloud heights of about 6,750 ft above mean sea level (sec. 2.3) was calculated for the 5 days. This average coverage around 2300 local time (l.t.) was found to be only about 25 percent of the magnitude of the value given in figure 10, at the same time. Therefore, all HRIR values were multiplied by four in constructing the plots in figure 11. Under the assumption that the cloud amounts vary linearly between data times, the fit of the HRIR data points into the pattern established by the ATS-3 observations offers further credibility to the procedure used.

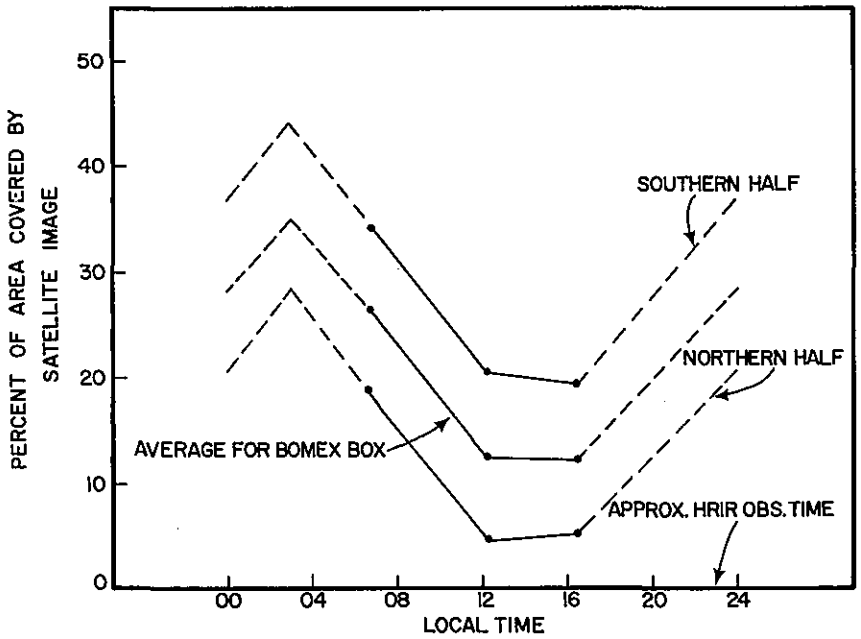

Figure 10.--Average diurnal variation in the percent area covered by satellite cloud image for the 5-day period.

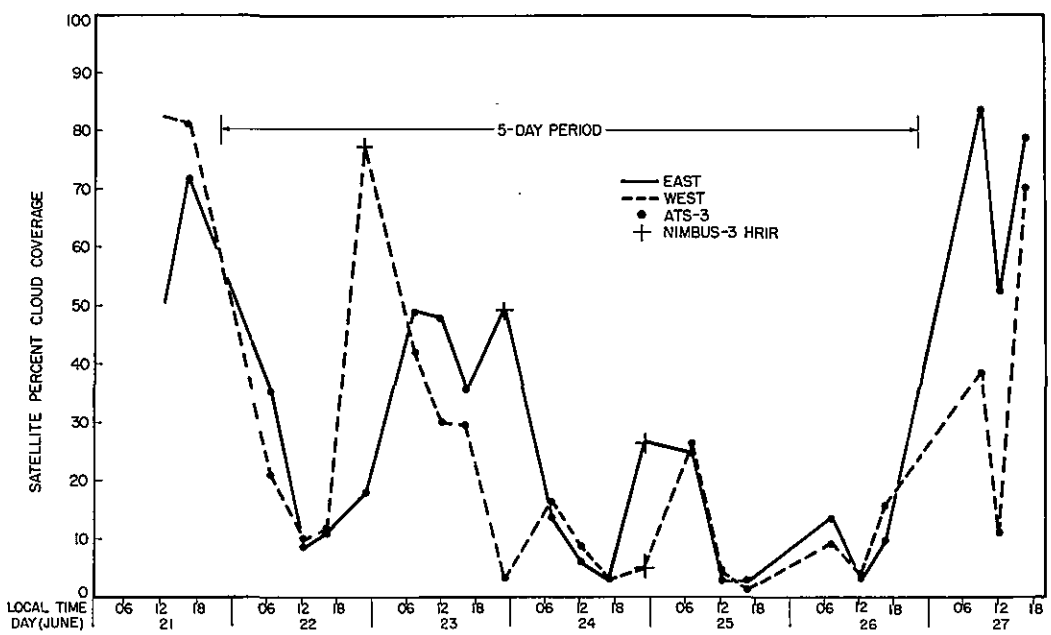

Figure 11.--Time plots of the percent of the eastern and western halves of the BOMEX square covered by satellite cloud image.

4.5 Summary of Steps Taken in Deriving Rainfall Estimates From Radar and Satellite Data

In deriving the rainfall estimates presented in section 5.3, the following steps, which are based on the procedures described in the preceding sections, were the principal ones:

(1) The lengths of all radar echoes falling within the BOMEX area covered by radar measurements were derived from the digital data for each observation time, and the echoes were grouped by radar and for ranges up to 100 mi and from 100 to 200 mi. Figure 12, which shows relative frequency distributions of radar echo lengths within 5 mi (8 km) class intervals for the 5-day undisturbed period and for several hours during the more disturbed periods just before and after the 5 days, summarizes the range of echo sizes observed for the analysis.

(2) The statistical model of precipitation echoes was used to derive $\overline{R}$--eq. (2)--for every observation time and for each area described under (1) above. For selected time periods and for radar ranges of less than 100 mi, rainfall estimates derived from the statistical model were compared with rainfall estimates obtained directly from the digitized gain-step data. Results of these comparisons are presented in section 6.3.4.

(3) Average rainfall rates were derived for successive 6-hr intervals by means of numerical trapezoidal integration.

(4) The 6-hourly rainfall estimates for the areas falling outside 100 mi were adjusted for non-beam filling according to the empirical procedure described in section 4.3.5.

(5) The 6-hourly rainfall estimates from the two radars were areally weighted and combined to give estimates for the entire southern half of the BOMEX volume.

(6) Based on the 6-hourly ratios of cloud coverage, estimated from ATS-3 and Nimbus-3 satellite data, the rainfall estimates were extended to the northern half of the BOMEX volume (sec. 4.4).

(7) The estimates for the northern and southern halves were combined to give rainfall estimates covering the entire BOMEX square.

5. DISCUSSION OF RESULTS

5.1 Rain-Gage Analysis

The results of the analysis from the shipboard rain-gages are plotted in figure 13. These values are accumulated amounts for the 3 hr immediately preceding the times shown on the abscissa, and are relative to the maximum accumulated value for June 21 from 1400 to 1700 l.t. Zeros and traces are omitted from the plot, and no data were missing until June 26 at 2000 l.t.

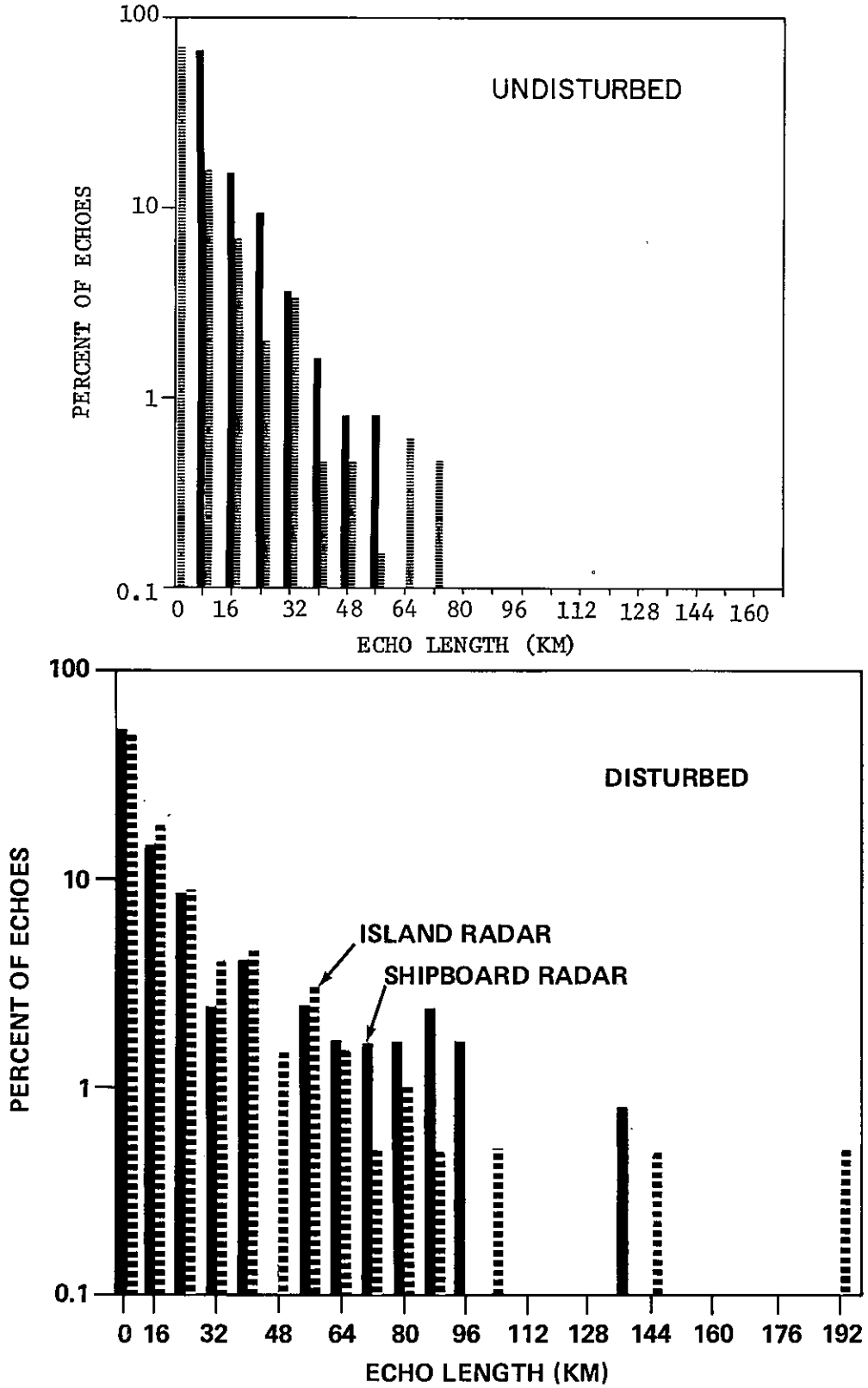

Figure 12.--Relative frequency histograms of echo lengths for the 5-day undisturbed period (top) and for several hours during the relatively disturbed periods just before and after the 5-day period (bottom).

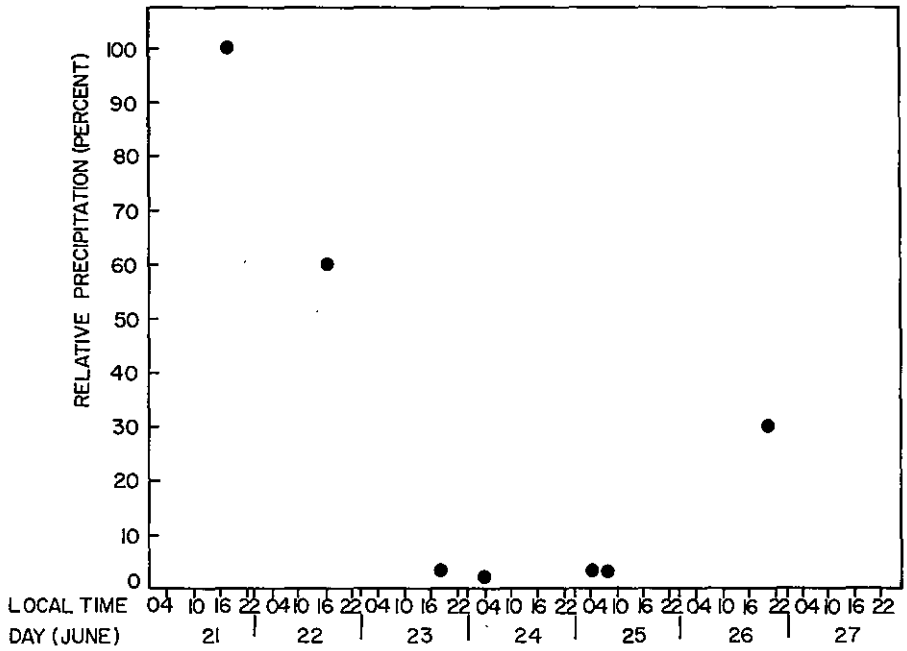

Figure 13.--Mean relative precipitation deposited over the BOMEX square at 3-hourly intervals as estimated from the five shipboard rain gages.

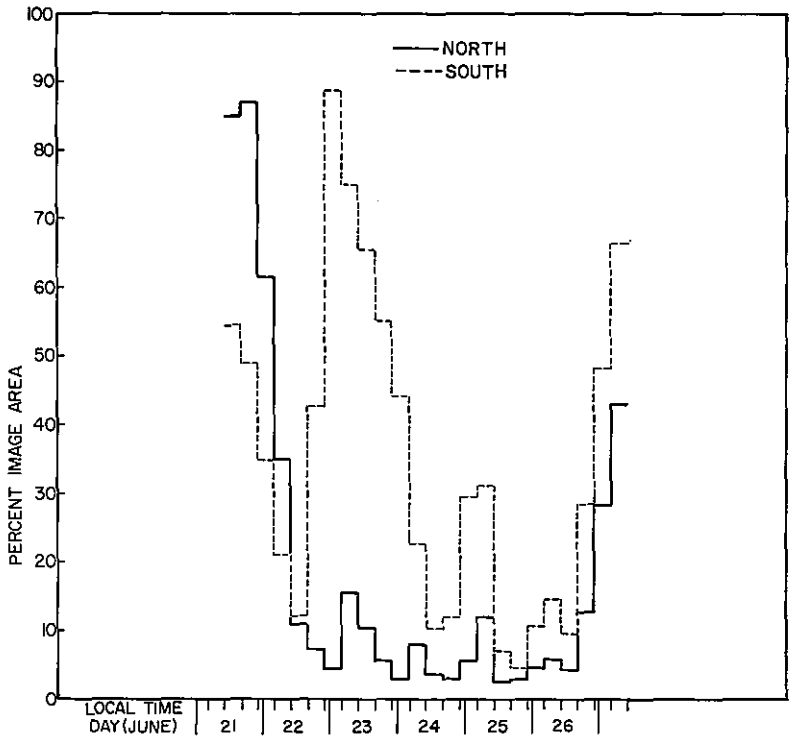

Figure 14.--Time plots of the percent of the southern and northern halves of the BOMEX square covered by satellite cloud image.

The results from the rain-gage analysis support the description of the weather systems presented in section 3, revealing relatively quiescent conditions during practically the entire 5 days, with noticeable increases in convective rainfall just before and immediately after the quiescent period. The value plotted at 1700 l.t. on June 22 reflects a significant accumulation observed only at the station occupied by the Mt. Mitchell at the southwest corner of the BOMEX square.

5.2 Space and Time Variations of Cloud and Echo Amounts

The time plots of cloud amounts derived from satellite data shown in figure 14 indicate consistently greater cloud coverage over the southern half of the BOMEX area than over the northern half, except at the very beginning of the 5-day period. Similar results are observed in the plot of radar echo amount versus latitude in figure 15, which shows that the average radar echo amounts decreased with increasing latitude. These results were derived from data collected with the island-based radar at ranges of 60 to 150 mi. The curve was constructed by processing data within range increments, under the assumption that any spatial variations in echo amount at a constant range results from latitudinal variation. Examining the data at a constant range provides a method of significantly reducing the uncertainty associated with comparing data at several different ranges with various degrees of non-beam filling. The non-beam filling problem is circumvented by this method to some extent, but figure 15 does not include any adjustment of the absolute numbers to account for non-beam filling.

Both island and ship radar data, adjusted for non-beam filling by using echo areas instead of rainfall as described in section 4.3.5, were used in deriving figure 16, which shows the percent of area within the BOMEX box covered by radar echo for 6-hr intervals during the 5 days. This figure does not reveal any east-west biases or differences that remain consistent for the 5 days. The larger echo coverage observed with the island radar on June 22 correlates with the result of the rain-gage analysis, which showed that a significant amount of rainfall was recorded aboard the Mt. Mitchell on June 22 (sec. 5.1).

The comparatively large echo coverage observed by the island radar from midday on June 25 to midday on June 26 results from numerous small echoes instead of from larger organized ones. Because echo size and rainfall are directly and nonlinearly related in this study through eq. (2), the rainfall estimates for this time period on June 25 and 26 remain relatively low in magnitude compared with those for other times during the 5-day undisturbed period (sec. 5.3). Conversely, a few large echoes that existed between 2200 l.t. on June 26 and 0400 l.t. on June 27 produced a measurable rainfall increase, although there was not a proportional increase in total areal echo coverages.

Figure 11 (sec. 4.4.2), which shows cloud coverage derived from satellite data, does not reveal any significant and persistent variations in cloud cover between the western and eastern halves of the BOMEX box. As

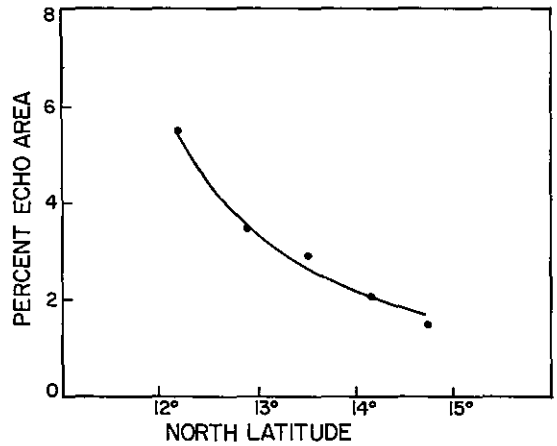

Figure 15.--Average percent echo coverage vs. latitude derived from island radar data for the 5-day period.

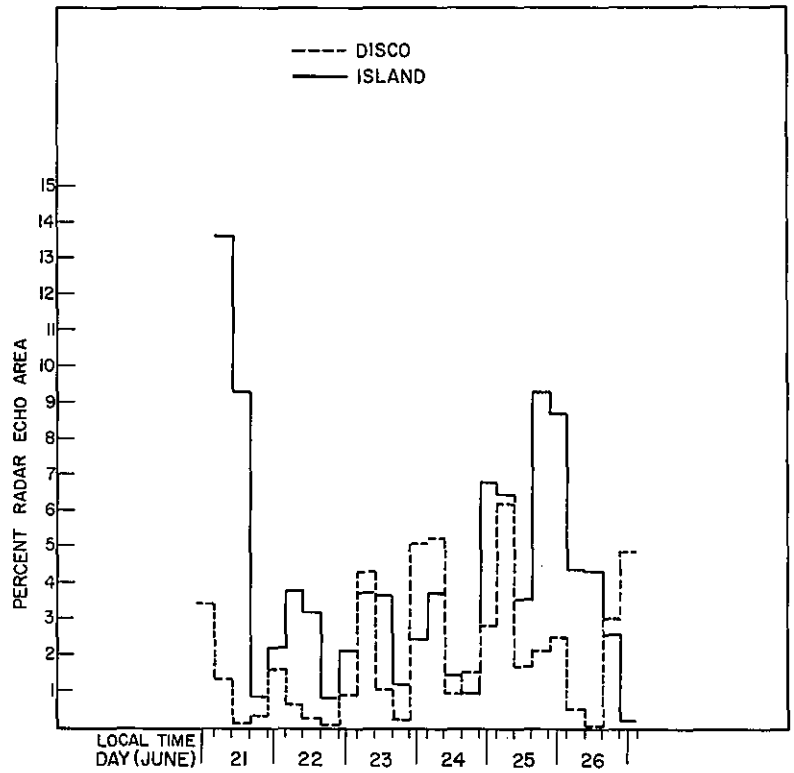

Figure 16.--Percent of areas inside the BOMEX square out to radar ranges of 200 mi that were covered by echo during the 5-day period.

expected, the cloud and echo coverage is greatest on the west side at the beginning of the period, when moderately disturbed weather was leaving that area, and on the east side at the end of the period, coincident with the arrival of a mild disturbance in the eastern part.

The average diurnal variation of echo coverages for the 5 days based on observations with the two surface-based radars is illustrated in figure 17. These and analogous curves for cloud amounts shown in figure 10 (sec. 4.4.2) reveal a minimum around midday and a maximum during the early morning hours. Inference for disturbed conditions should not be made from these results. Radar echo statistics derived from BOMEX data for both disturbed and undisturbed weather, comparisons of diurnal variations for both these conditions, and physical interpretations of such variations are discussed in an earlier publication (Hudlow, 1970b).

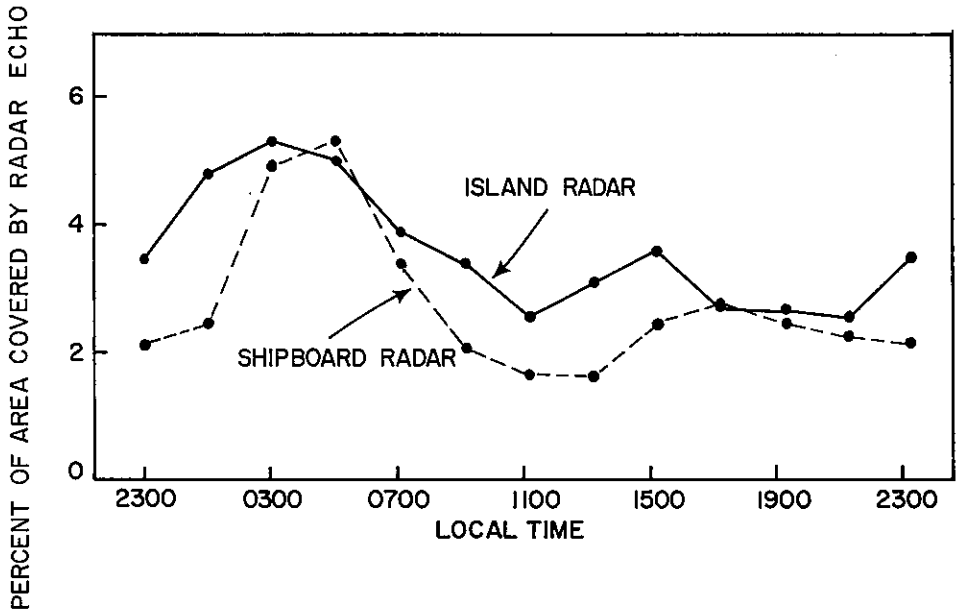

Figure 17.--Average diurnal variation in radar echo amounts over the portions of the BOMEX square viewed by each radar during the 5-day period.

5.3 Six-Hourly, Daily, and 5-Day "Best Estimates" of Rainfall Amounts

The results from the quantitative precipitation analysis, as derived from radar and satellite data by the procedures described in the preceding sections, are summarized in the bar graph in figure 18, showing average rainfall rates over the entire BOMEX box for 6-hr intervals. The average rainfall rate for the entire 5-day period is only about 0.35 mm/day and the greatest 24-hr total, which is approximately equal on both June 25 and June 26, is estimated at 0.5 mm. These results give further evidence that the 5 days can be characterized as undisturbed.

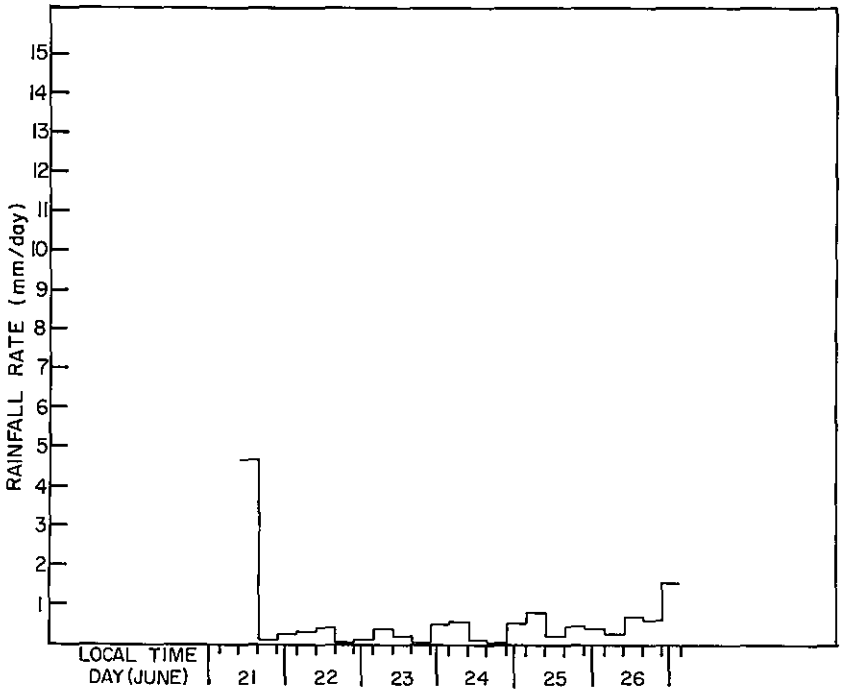

Figure 18.--Bar graph of 6-hourly estimates of the average rainfall rate over the BOMEX square as derived from radar and satellite data.

Figure 18 also illustrates that the period under study was immediately preceded by a moderately intense disturbance and followed by a mild disturbance, which produced average rainfall rates of about 4.7 mm/day and 1.5 mm/day, respectively, during the two most intense 6-hr intervals.

5.4 Comparison of Results With Previous Studies

A search of the literature uncovered a published study on quantitative radar measurements in the vicinity of Barbados by Saunders (1965), who analyzed radar data for several echoes observed from the island with an M-33 radar. He concludes from an examination of the M-33 radar and island rain-gage data that rainfall rates in excess of 100 mm/hr at a point for as long as a few minutes are not extremely rare. This compares favorably with the BOMEX radar data analysis. For example, from results based on the statistical echo model, it can be shown that peak rainfall intensities of about 85 mm/hr at a point accompany an echo size $D \approx 35$ mi, the echo size that produces the greatest percentage of the rainfall. For an echo of this same size, the statistical model gives an average rainfall rate, for an instant in time, over the total echo area of one thirty-fifth that of the peak, or about 2.5 mm/hr. The statistical model yields a practical upper limit for point rainfall rates of about 300 mm/hr, corresponding to an echo length of about 100 mi. This result agrees favorably with the highest 1-min rain rates accompanying the drop-size distribution observed in Majuro, Marshall Islands, by Mueller and Sims (1969), the distribution adopted for the BOMEX analysis (sec. 4.3.1).

6. ASSESSMENT OF ERRORS

The rainfall estimates given in section 5.3 are subject to errors inherent in the rainfall derivations. Sufficient information is not available to precisely establish the magnitudes of these errors, but based on results from other studies, and by considering additional factors unique to BOMEX, it is possible to ascertain mean lower and upper confidence limits for the estimates.

6.1 Error Expected Under Standard Operational Conditions

Based on the findings by previous investigators, it is possible to assess the average error accompanying radar precipitation measurements if the following standard operational conditions are fulfilled:

(1) Equipment capable of stable and reliable measurements is used.

(2) Suitable calibration, sampling, and processing procedures are applied.

(3) Areas of measurement are restricted to ranges of less than 80 mi.

(4) Attenuation caused by rainfall is small.

(5) Seasonal adjustment is applied to the radar data based on a comparison with drop-size and/or rain-gage data.

Two experiments conducted under conditions that largely satisfy the five criteria described above have produced sufficient data to perform statistically significant error analyses. One of the experiments, carried out by the Valdai Hydrological Research Laboratory in the USSR, is especially pertinent here, since, as in BOMEX, X-band radar was used. The other study, by Wilson (1970a), was done with S-band radar data and attenuation effects were, therefore, negligible.

Borovikov et al. (1970) report on results derived from an analysis of a comprehensive set of 3-cm radar data and rain-gage data collected during 1964 and 1965 in the Valdai region for several proving grounds ranging in size from 100 to 8,600 km^2. They conclude that, within ranges of 80 km, rainfall estimates can be derived from radar data with the average error held to within 40 percent for storm totals of 1 mm or more and areal averages over 100 km^2 or greater. In achieving this accuracy, seasonable adjustments were applied to the radar data by comparing the seasonal rainfall estimates based on those data with climatological rain-gage network measurements, a procedure similar to the one used here (sec. 4.3.2).

In his detailed comparison of 10-cm radar data with rain-gage data, Wilson (1970a) analyzed 28 events from 4 years of thunderstorm data. He used radar data collected by the staff at the National Severe Storms Laboratory (NSSL), Norman, Okla., for comparison with rainfall amounts recorded by a dense rain-gage network maintained by personnel at the Agricultural Research Service (ARS), Southern Plains Watershed Research Center. The ARS rain-gage

network, which lies within 70 mi of the NSSL radar, covers a 1,000-mi^2 area and has an average density of one gage per 8 mi^2.

The tabular results presented by Wilson yield an average percent error, $\overline{p}$, of about 50 for the storm totals. The percent error is defined as

$$p = \frac{|(T - E)|}{T} \times 100 \quad , \tag{8}$$

and the average percent error is given by

$$\overline{p} = \sum_{i=1}^{n} \left(\frac{|T_i - E_i|}{T_i n} \right) , \tag{9}$$

where T is the true value (in this instance taken to be the observed value from the dense ARS network), E is the radar estimate, and n is the number of events included in the error analysis. As in the study reported by Borovikov et al. (1970), all the events included from Wilson's analysis pertained to storm totals of 1 mm or greater.

From eq. (9) and the results of the error analysis based on Wilson's data, estimates for the mean upper and lower confidence limits, within which approximately 70 percent of the radar estimates lie, are given by:

$$\text{UPPER} = \frac{100\ E}{100 - \overline{p}} \quad , \tag{10}$$

and

$$\text{LOWER} = \frac{100\ E}{100 + 1.15\ \overline{p}} \quad , \tag{11}$$

where the 1.15 in the denominator of eq. (11) results from skewness in the distribution of errors, i.e., there is a greater tendency to underestimate than to overestimate the rainfall from radar. Using Wilson's $\overline{p} = 50$, which does not differ appreciably from the value of 40 reported by Borovikov et al., gives

$$\text{UPPER} = 2\ E \quad , \tag{12}$$

and

$$\text{LOWER} = 0.63\ E \quad . \tag{13}$$

An approximate way of stating this result is: "Under standard operational conditions the radar estimate is in error, on the average, by a factor of 2." It is possible to attain higher average accuracy by continually incorporating drop-size and/or rain-gage data with the radar data. However, independent data suitable for this purpose were not collected during BOMEX.

6.2 Sources of Error

The magnitude of the error accompanying rainfall estimates derived from radar data depends on the type of equipment, calibration procedures,

data collection frequency, data processing procedures, the degree of non-beam filling, unknown alterations in the R versus Z_e relationship due to variations in the drop-size distribution, and the intensity of the precipitation. The magnitude of the error from some of these sources, particularly variability of the R versus Z_e relationship and sampling, can be lowered appreciably through spatial averaging and/or temporal integration, an approach especially suitable for many hydrologic applications, including the one considered here, since obtaining the average amount of precipitation deposited over a specified area during a given time interval is often the objective.

Wilson (1970b), using the same sources of data as those described in the preceding section, examined the effect of the sampling frequency and the size of the area on the average error incurred in deriving areal estimates of rainfall from radar data. Figure 19 summarizes the results from this aspect of his analysis. It illustrates that as the area and the sampling frequency increase, the portion of the error that is dependent on the sampling rate and the scale of averaging decreases.

As stated earlier, another consideration in assessing the error accompanying rainfall estimates from radar is the intensity of the rainfall being measured. Generally, it has been observed that the relative error decreases as the amount of precipitation increases. All the reasons for this trend are not clear, but there is evidence that a decrease in error in the rainfall estimates partly results from a relative decrease in error in the R versus Z_e relationship at higher rainfall rates. This implies that the greater the rainfall rate, the less variable is the drop-size distribution. Another consideration is storm duration and area, which are positively correlated with total storm rainfall. Storms of long duration provide a greater time interval for temporal integration of nonzero values, which statistically should result in a lower overall error. Similarly, as illustrated by figure 19, the error decreases as the area used for averaging increases. Figure 20 shows the results from a least-squares fit to Wilson's (1971) tabular data. Equation (8) defines percent error. Figure 20 illustrates the effects of rainfall amount on the percent of error in precipitation estimates for this set of radar data.

6.3 Errors Characteristic of BOMEX

Based on preceding evidence and the conditions described, it follows that the BOMEX radar precipitation estimates may be in error, on the average, by at least a factor of 2.0. However, additional sources of error unique to BOMEX and related to the standard operational conditions enumerated in section 6.1 need to be examined for the purpose of establishing expected upper bounds on the error accompanying the precipitation estimates. The important question here is: What maximum additional uncertainty, beyond the base or standard factor of 2.0, may be added because of the characteristics of the BOMEX data set? To be considered in answering this question are the following:

(1) Overall calibration procedures.

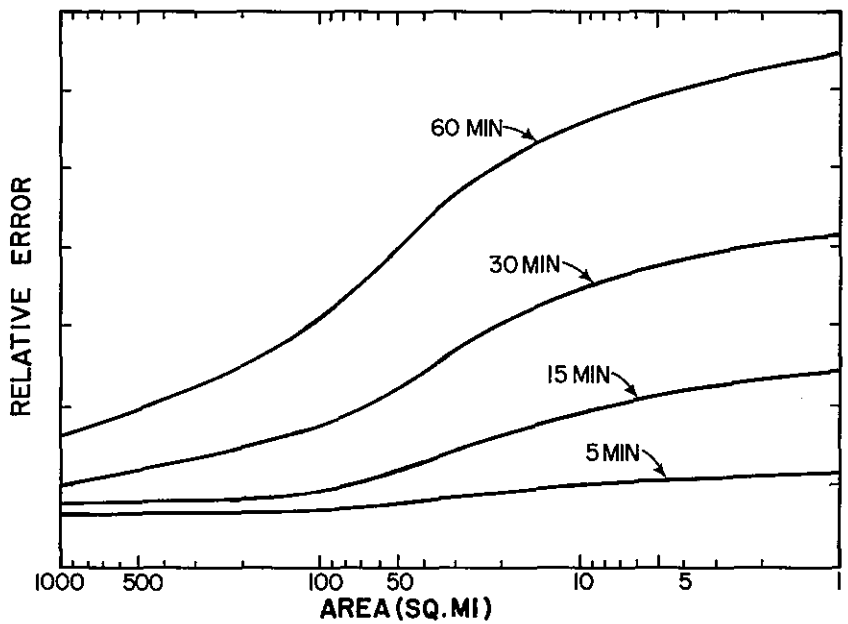

Figure 19.--Relative error for storm rainfall estimates as a function of time between radar data samples and size of area for convective thunderstorms in the Oklahoma area (derived from Wilson, 1970b, p. 13).

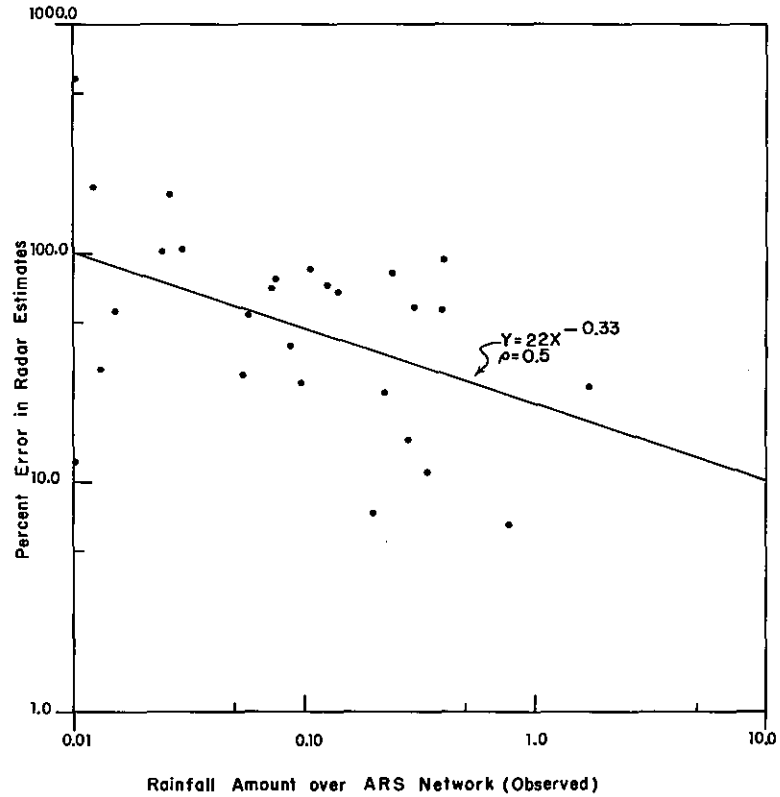

Figure 20.--Percent error in 3-hourly storm rainfall estimates derived from WSR-57 radar data for a 1,000-mi^2 watershed in Oklahoma vs. rainfall amount derived from data presented by Wilson (1971, p. 21).

(2) Sampling errors.

(3) Attenuation by liquid water.

(4) Accuracy of the statistical echo model.

(5) Adjustment for non-beam filling.

(6) Extrapolation via satellite data.

6.3.1 Overall Calibration Procedures

As explained in section 4.3.2, the general approach adopted for calibrating the BOMEX radar data included a comparison of radar data with island rain-gage data for several storms. An average adjustment (calibration) factor was calculated, which was assumed constant for all times and oceanic areas considered in this analysis. Inherent in this assumption are two shortcomings: (a) hardware calibrations might differ from those that would apply during the storms used for the comparison and (b) the relationship of R versus Z_e might be different, because of variability in space and time, from the one used during the comparison. Although the first difficulty was largely overcome through the conventional hardware and film calibrations performed daily in the field (Hudlow, 1970a), unknown changes in the standard calibration signal and human error may result in uncertainties.

As for the second problem, variations in the distribution of rain-drop sizes will alter the R versus Z_e relationship, and such variations occur in space and time. An explicit accounting for drop-size variations is not possible, but evidence presented in section 6.2 shows that the errors are substantially reduced by averaging the rainfall in space and/or integrating in time.

For BOMEX, the radar data were calibrated against rain gages located on the island of Barbados and were subsequently used to make rainfall estimates over oceanic areas at appreciable distances from the calibration area. Generally, it is risky to calibrate oceanic radar data through comparisons with rain-gage data over land, because "island effects" can alter the cloud physics and thus the drop-size distributions associated with the rainfall. The supposition made here is that storms originating at least 60 mi east-southeast of the island and moving into the rain-gage network will not be modified appreciably due to "island effects" prior to sampling. The storms selected for the radar/rain-gage comparisons satisfied the criterion of being of oceanic origin. It is concluded, therefore, that the uncertainty associated with using the island rain-gage network for calibrating the BOMEX radars is probably no greater than that normally associated with the calibration of radar, and that the BOMEX calibration procedures do not add significant additional error to the rainfall estimates.

6.3.2 Sampling Error

As illustrated in figure 19, the magnitude of the sampling error is a function of the sampling frequency and the scale used for spatial averaging

For BOMEX, the averaging area is several thousand square miles, which is more than ample for minimizing error through spatial averaging, but the average sampling frequency for the 5-day analysis presented here was only one sample every 45 min from the island radar and one sample every 75 min from the shipboard radar.

One of the reasons that a greater sampling frequency was not possible was the dual data collection requirement imposed on the ship radar. During specified periods precipitation surveillance was interrupted, and the shipboard radar was used for tracking weather balloons released from the deck of the ship. The interruption usually lasted at least 30 min and sometimes appreciably longer. After a visual inspection of many radar photographs collected during BOMEX, a subjective conclusion reached by the author is that even for an area as large as the BOMEX square, the interval between data collection should not exceed about 30 min because of the highly transient nature of tropical precipitation and because a short time interval should help minimize boundary errors. It is possible, for example, for radar echoes to move across only one corner of the BOMEX square in a relatively short time and for this activity to go unrecorded unless the data collection interval is short enough to resolve these occurrences.

It follows from the foregoing that the sampling frequency for the 5-day analysis was less than optimum. Yet, according to the curves shown in figure 19, the average error resulting from deficient temporal sampling should remain low, even for sampling intervals up to 1 hr, because of the large areas used in the BOMEX analysis. Therefore, additional errors in the 6-hr estimates, arising from inadequate temporal sampling, are assumed negligible compared with the magnitude of the total error.

6.3.3 Attenuation by Liquid Water

Attenuation resulting from liquid water was negligible during the 5-day period because undisturbed weather conditions prevailed. The number of points at which instantaneous attenuation corrections, derived by the procedures outlined in section 4.3.4, exceeded 1 dB were insignificant. The portion of the error in the point estimates attributable to liquid-water attenuation is in most cases a small fraction of 1 dB (1 dB $\approx$ 25 percent); therefore, this source of error is negligible in deriving the areally averaged estimates of precipitation.

6.3.4 Accuracy of the Statistical Echo Model

The quantitative rainfall estimates for the 5-day period and for areas inside the southern half of the BOMEX square were derived from the statistical echo model, which relates rain rate to echo length, rather than obtained directly from gain-step measurements. To examine how closely they would match, rainfall estimates derived by both methods were compared for four 6-hr periods covered by reliable gain-step data. The comparisons are based on 6-hr averages for a 3,000-mi^2 area contained within 100 mi of the island radar. Twelve of the 24 hr are at the beginning of the 5-day period (June 22) and the

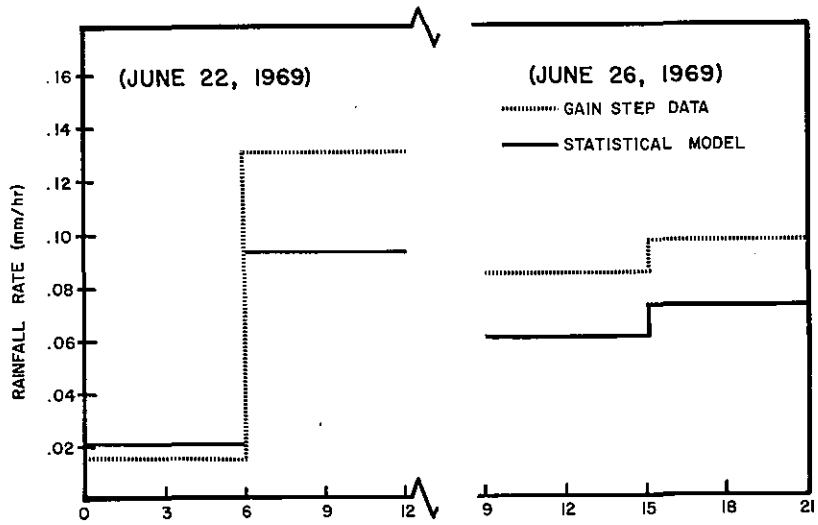

Figure 21.--Average rainfall rates over a 3,000-mi^2 area for 6-hr intervals derived from the statistical echo model compared with those obtained directly from digitized "gain-step" data.

other 12 at the end (June 26). Figure 21 shows the results from this comparison and indicates a 30-percent average difference between the precipitation estimates derived directly from the digitized gain-step data and those from the echo model. The average difference should decrease as the averaging area and/or the number of computational periods increase. As seen in figure 21, the statistical echo model gave underestimates, compared with the gain-step data, for three of the four 6-hr periods and an overestimate for the remaining 6-hr period.

These two methods of estimating rainfall from radar were also compared for three 6-hr periods on June 29 that were relatively disturbed by organized convection. Results showed no differences exceeding 30 percent (Hudlow and Scherer, 1975). For one of the three periods on June 29 there was agreement, for one the statistical model gave an overestimate, and for the third the model yielded an underestimate. The algebraic sum of the error in percent was zero.

Based on these comparative analyses for June 22, 26, and 29, it is concluded that the portion of the error in any 6-hr estimate (sec. 5.3) attributable to the use of the echo model is likely not to exceed 30 percent. It further appears that the error is reduced to less than 20 percent for the daily estimates and to a negligible amount for the 5-day estimate.

6.3.5 Adjustment for Non-Beam Filling

As described in section 4.3.5, there exists, to a first approximation, east-west spatial homogenity in the precipitation averages for the 5-day period. It is concluded that no additional error is introduced into the

precipitation estimate for the entire 5 days as a result of the empirical adjustment procedure for non-beam filling, which invokes this hypothesis. However, errors are incurred when the procedure is applied to shorter time intervals within the 5-day period. The purpose of this section is to place upper bounds on the magnitude of these errors in terms of (1) daily estimates and (2) 6-hourly estimates.

The approach used to adjust for non-beam filling at ranges beyond 100 mi consists of multiplying the unadjusted 6-hr estimates of precipitation by a single adjustment factor for each radar:

$$F_{1,2} = \frac{\left[\sum_{i=1}^{20} E_i\right] : \quad r \leq 100 \text{ mi}}{\left[\sum_{i=1}^{20} E_i\right] : \quad r > 100 \text{ mi}} , \tag{14}$$

where F_1 and F_2 are the adjustment factors for the island and shipboard radars, respectively, and E_i is the unadjusted precipitation estimate for each of the 6-hr periods within the 5 days.

The magnitude of the error associated with adjusting the precipitation estimates for non-beam filling, by means of the expression

$$E_{adjusted} = \left(E_{unadjusted}\right)\left(F_{1,2}\right) , \tag{15}$$

is related to the length of the computational time period, Δt, and the upper bound for this source of error can be appraised by considering the temporal distribution of F at a time resolution equivalent to Δt. Table 3 gives daily values of F for the 5 days for both radars, the mean F for the 5-day period being 5.5 for the island and 13.5 for the shipboard radar.

Table 3 illustrates two important features: (a) all daily values of F are substantially greater than 1, and (b) the largest percent difference between a daily F value and the 5-day value is 45 percent for the island radar and 63 percent for the shipboard radar. Thus, the daily F values are reasonably consistent with the 5-day values. Based on the data in table 3, it is concluded that for all daily estimates of precipitation contained within the 5-day period considered here, an F adjustment of at least 3.5 and 5.0 should be applied, which corresponds to the minimum F value for the island and shipboard radars, respectively. Furthermore, it is expected that the probable maximum error, which will be incurred by applying the 5-day mean F to all daily estimates, will not exceed that corresponding to the largest percent difference shown in table 3: 45 percent for the island and 63 percent for the shipboard radars.

An approach analogous to the one just presented for the daily estimates can be used for the error analysis of the 6-hourly estimates. Table 4 gives relative frequency distributions of the 6-hourly F values for each radar, and reveals, as expected, more variability in these distributions than was

Table 3.--Daily ratio, derived by dividing the radar estimates of daily precipitation for that portion of the BOMEX square within a range of 100 mi by those for the area outside 100 mi, and percent differences between the daily ratios and the 5-day mean ratios

Date (1969)	Local time (l.t.)	Island Radar F	Island Radar Percent Difference	Shipboard Radar F	Shipboard Radar Percent Difference
June 21-22	2200-2200	6.5	18	14	4
June 22-23	2200-2200	3.5	36	18	33
June 23-24	2200-2200	6.0	9	5	63
June 24-25	2200-2200	8.0	45	9	33
June 25-26	2200-2200	4.2	23	22	63
	Mean	5.5	Mean	13.5	

Table 4.--Relative frequency distributions of 6-hourly ratios (F's) and percent differences between these ratios and the 5-day mean ratios

Island Radar F	Island Radar Cases (percent)	Island Radar Difference (percent)	Shipboard Radar F	Shipboard Radar Cases (percent)	Shipboard Radar Difference (percent)
< 1	5	82	< 1	6	93
1 - 2	5	73	1 - 4	14	82
2 - 4	35	45	4 - 8	20	56
4 - 6	10	9	8 - 12	20	26
6 - 8	5	27	12 - 16	0	4
8 - 10	20	64	16 - 20	0	33
>10	20	82	20 - 24	8	63
			24 - 26	8	85
			>26	24	93

observed in the daily distributions. For the island radar, 75 percent of the 6-hourly ratios observed during the 5 days are within 82 percent of the 5-day ratio. For the shipboard radar, 70 percent of the 6-hourly ratios are within 93 percent of the 5-day ratio. By relating an upper threshold of percent

difference to the same percent of the cases for both radars, the results shown in table 4 can be restated approximately as follows: 75 percent of the 6-hourly ratios observed during the 5 days with the island radar are within 80 percent of the 5-day ratio, while 75 percent of those observed with the shipboard radar are within 100 percent of the 5-day ratio. It follows that the probable maximum error from this source for 75 percent of the 6-hourly estimates will not exceed that corresponding to the upper threshold percentages of 80 and 100, respectively, for the areas covered by the island and shipboard radars.

6.3.6 Extrapolation With Satellite Data

One weakness of the procedure described in section 4.4.1 for using satellite data to extrapolate radar precipitation estimates from the southern half of the BOMEX box is that all cloud types discerned by the satellite were not necessarily precipitating. If the cloud types in the north were different from those in the south, then error can occur in the method used for extrapolation. However, since cloud amounts were significantly smaller in the north than in the south during the 5 days, except at the very beginning of the period, the extrapolation is in a stable direction. This becomes apparent from examination of table 5, which contains estimates of (1) rain rates over the southern half of the BOMEX square, (2) the north/south satellite cloud ratios, (3) rain rates over the northern half of the BOMEX square, and (4) rain rates over the entire BOMEX square. The mean of the north/south satellite cloud ratios for the 5-day period is 0.45.

As in the case of non-beam filling, the purpose here is to estimate the upper bounds of error magnitude in terms of daily and 6-hourly estimates.

The data in table 5 illustrate that the largest daily north/south satellite cloud ratio for the 5 days is about 1.0, which occurred on the first day of the period. A reasonable assumption for undisturbed weather conditions, such as those which prevailed during the 5 days, is that the maximum error attributable to extrapolation of satellite data would result if all clouds observed over the northern half of the BOMEX square produced no precipitation while precipitation was observed over the southern half during the same period. Under these conditions, the error introduced into the daily precipitation estimates from extrapolation to the total area would be a factor of 2 for the first 24 hr of the 5-day period and considerably less for the other 4 days.

Examination of table 5 also reveals that the ratio for which 75 percent of the 6-hourly ratios do not exceed the 5-day mean ratio is 0.5. Therefore, the maximum additional error introduced into the 6-hourly precipitation estimates for the entire BOMEX box by the extrapolation procedure would not exceed a factor of 1.5 for 75 percent of the 6-hr periods.

6.3.7 Summary of Probable Confidence Limits

Figure 22 illustrates the portion of the BOMEX square that was covered by (1) radar measurements at ranges inside 100 mi, (2) radar measurements at ranges beyond 100 mi, and (3) satellite measurements. In this figure, A_1 and

Table 5.--Estimates of 6-hourly average rain rates and north/south satellite cloud ratios

Date (1969)	Local time (l.t.)	Southern half (mm/day)	North/south satellite ratio	Northern half (mm/day)	Entire BOMEX square (mm/day)
June 22	2200-0400	0.16	1.7	0.27	0.22
"	0400-1000	0.21	1.6	0.34	0.28
"	1000-1600	0.43	0.9	0.39	0.41
"	1600-2200	0.03	0.2	0.01	0.02
June 23	2200-0400	0.12	0.05	0.01	0.06
"	0400-1000	0.63	0.2	0.13	0.38
"	1000-1600	0.27	0.2	0.05	0.16
"	1600-2200	0.04	0.1	0.01	0.02
June 24	2200-0400	0.97	0.1	0.10	0.53
"	0400-1000	0.90	0.3	0.27	0.58
"	1000-1600	0.09	0.3	0.03	0.06
"	1600-2200	0.09	0.2	0.02	0.05
June 25	2200-0400	0.90	0.2	0.18	0.54
"	0400-1000	1.18	0.4	0.47	0.83
"	1000-1600	0.29	0.4	0.12	0.20
"	1600-2200	0.58	0.6	0.35	0.46
June 26	2200-0400	0.63	0.4	0.25	0.44
"	0400-1000	0.39	0.4	0.16	0.27
"	1000-1600	1.00	0.4	0.40	0.70
"	1600-2200	0.87	0.4	0.35	0.61

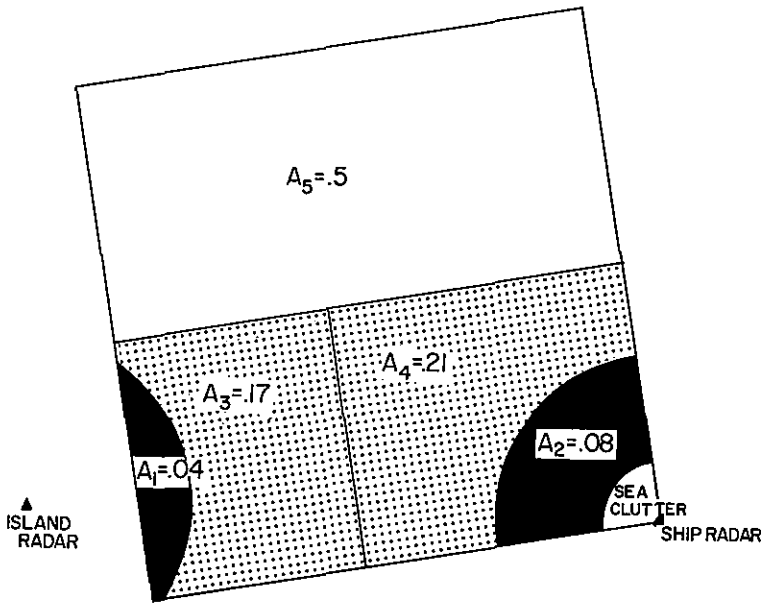

Figure 22.--Portions of the BOMEX square covered with radar measurements at ranges within and beyond 100 mi, and the portion covered only by satellite data.

A_2 refer to the fractions of the BOMEX square that fell within 100 mi of the island and shipboard radars, respectively; A_3 and A_4 to the portions covered by the island and shipboard radars, respectively, at ranges beyond 100 mi; and A_5 to the fraction for which satellite coverage was available. In the discussion that follows, A_T ($A_1 + A_2 + A_3 + A_4 + A_5 = 1.0$) is used to denote the total of these fractions.

Table 6 gives the average error (error factor = 2.0), that can accompany the BOMEX rainfall estimates under standard operational conditions and the probable maximum error that might accompany the daily 6-hourly and 5-day estimates, in the worst case, for various portions of the BOMEX square. For example, daily rainfall estimates for the southern half of the area would probably be in error, on the average, by approximately a factor of 2.0. The estimate for a specific day could be in error by a greater or lesser amount but should not exceed a factor of 3.3 for the estimates over the southern half.

The derived error factors contained in table 6 are in terms of their sources, as follows:

(1) e_b = expected standard or base error under standard operational conditions;

(2) e_m = maximum probable error due to the application of the statistical echo model;

(3) e_n = maximum probable error due to inaccuracies in the procedure for applying non-beam filling corrections to the radar data at ranges beyond 100 mi; and

(4) e_s = maximum probable error due to uncertainties in the technique used to derive precipitation estimates over the northern half of the BOMEX square from satellite data.

Table 6.--Summary of confidence limits, expressed as error factors, for BOMEX precipitation estimates

Sections of BOMEX area	Average limits under standard conditions	Probable upper limits for BOMEX conditions		
		6-hourly (75% of cases)	Daily	5-day period
A_1 and A_2	2.0	2.6	2.4	2.0
A_3	2.0	4.6	3.4	2.0
A_4	2.0	5.2	3.9	2.0
$A_1 + A_3$	2.0	4.2	3.2	2.0
$A_2 + A_4$	2.0	4.4	3.5	2.0
$A_1 + A_2 + A_3 + A_4$	2.0	4.3	3.3	2.0
A_T (total area)	2.0	6.4	5.0	2.5

In table 6, all magnitudes are expressed as a factor (multiple) of the true value. Thus, an error factor of 2.0 means that the estimate can be a factor of 2 in error, or that it can be as large as 2 times or as small as 1/2 the true value. The following example, pertaining to the daily estimates (d) for the area covered by the island radar ($A_1 + A_3$), illustrates the manner in which the error factors contained in table 6 were derived. The error components in this example are:

$e_b = 2.0$ = expected standard, or base, error factor for standard operational conditions,

$e_{md} = 1.2$ = maximum probable error factor due to the application of the statistical echo model for deriving daily precipitation estimates, and

$e_{nd} = 1.45$ = maximum probable error factor due to inaccuracies in the procedure for applying non-beam filling corrections, at radar ranges beyond 100 mi, for the daily precipitation estimates.

Based on these error components, the estimate for the total error factor pertaining to the area $A_1 + A_3$ is given by

$$\frac{\left[(e_b \cdot e_{md})\ A_1 + (e_b \cdot e_{md} \cdot e_{nd})\ A_3\right]}{(A_1 + A_3)} . \tag{16}$$

Substituting the numerical estimates for the error components and the areal fractions into eq. (16) gives

$$\frac{\left[(2 \times 1.2)(0.04) + (2 \times 1.2 \times 1.45)(0.17)\right]}{(0.04 + 0.17)} = \approx 3.2.$$

Table 6 shows that the probable upper limit of the error increases as the time interval decreases, primarily as a result of the procedure used in adjusting for non-beam filling, since the principal assumption involved becomes less valid for shorter time periods (sec. 4.3.5). The increase in the probable upper limit of the error for the total BOMEX square, over that for the southern half only, arises from uncertainties accompanying the procedures for extrapolating satellite data to the northern half.

The substantially larger BOMEX averaging area could lower the base error factor: thousands of square kilometers compared with the hundreds of square kilometers for which the base error factor of 2.0 was derived. This might explain the findings by Hudlow and Scherer (1975), who show that, by making independent evaporation computations with a bulk aerodynamic model and solving for precipitation from the atmospheric water budget residual, the error accompanying the radar/satellite precipitation estimate for the 5-day period probably is significantly less than the confidence limits in table 6.

Using the upper confidence limits given in table 6 for A_t (daily and 5-day), it is concluded that an atmospheric water budget analysis for the 5 days would yield errors in the evaporation estimates, originating from errors in the precipitation estimates, of less than 25 and 12 percent for the daily and the 5-day estimates, respectively. This assumes an evaporation rate of roughly 7 mm/day and a precipitation rate of 0.35 mm/day.

7. CONCLUDING REMARKS

BOMEX radar, satellite, and rain-gage data were used in this study for describing the precipitation morphology for a 5-day period characterized by undisturbed weather conditions. The techniques used, and conclusions drawn, may not apply to disturbed weather. For example, a diurnal variation of convection over the BOMEX oceanic areas is not as evident during undisturbed periods. On the other hand, the error analysis presented in section 6 has, at least in part, general applicability. It should be expected that the percent error in the X-band radar estimates will increase during disturbed conditions, since errors arising from liquid water attenuation will increase with greater rainfall rates. However, relative errors due to non-beam filling will decrease significantly during disturbed conditions, when the statistical echo model is used for estimating rainfall amounts, offsetting part of the increase in error from liquid-water attenuation.

Some specific conclusions inferred from this study period are:

(1) The 5-day period was characterized by undisturbed weather conditions, immediately preceded and followed by moderate and mild disturbances, respectively, which were produced by tropical waves first identified over the African continent.

(2) On the average, minimums of echo amount were observed around midday, while maximums occurred in the early morning hours, and there is evidence that cloud amounts also followed this pattern.

(3) On the average, echo and cloud amounts were observed to decrease with increasing north latitude.

(4) Cloud and echo coverages were greatest over the western half of the BOMEX square early in the period and over the eastern half at the end of the period, and during most of the 5 days no significant and persistent east-west variations were detected.

(5) A statistical relationship between rainfall rate and echo size (length) gives estimates of rainfall rate that compare favorably with those derived directly from digitized gain-step data and with rates reported by other investigators. The echo model shows that a large portion of the precipitation content within a tropical convective echo, at an instant in time, is distributed over a relatively small portion of the echo area.

(6) Quantitative rain-rate estimates derived for time intervals as short as 6 hr for the BOMEX square reveal that (a) the average rainfall rate for the 5 days is about 0.35 mm/day and (b) the largest 24-hr total, about equal on both June 25 and June 26, is 0.5 mm.

(7) Estimates for the mean rain rate over the entire BOMEX square are expected to be in error, on the average, by a factor of 2 or more. The error factors for a specific time period may be larger or smaller than 2.0, but will not exceed, in the worst cases, 5.0 and 2.5 for the daily and 5-day estimates, respectively.

(8) Considering the magnitudes of the quantitative rainfall estimates and the expected confidence limits placed on these estimates and through independent comparisons from atmospheric budget analysis, it is concluded that daily precipitation was less than 25 percent of evaporation (evaporation rate $\approx$ 7 mm/day) and that the 5-day total precipitation was less than 12 percent of the total evaporation for the 5 days.

The greatest deficiency in the BOMEX precipitation data base results from the incomplete coverage of the BOMEX square with quantitative radar measurements. This deficiency was partly overcome by extending the radar data to far ranges by using a statistical model of radar echoes and an empirical adjustment for non-beam filling and by extrapolating with satellite data over areas not covered by radar. Applying these extensions to the data make it possible to derive quantitative rainfall estimates for the entire BOMEX

square, but at the expense of increasing the expected errors. In future experiments, great emphasis should be placed on acquiring complete spatial coverage of the experimental area with quantitative radar measurements. Ideally, the radar network should consist of radars with 5 cm or longer wavelengths and 1.75° or smaller beam widths. A sufficient number of radars should be available to cover the experimental area, with the radars spaced no further apart than about 175 km.

ACKNOWLEDGMENTS

The author is grateful to Wolfgang Scherer for technical assistance and many invaluable scientific consultations, and to Joshua Holland and Vance Myers for overall direction in the preparation of this study. Considerable help in basic data reduction was provided by Bill Stevens and Briah Connor, with the latter also assisting in the reproduction of the radar and satellite photographs. Thanks are also due Mike Divilio and Bryce Winn, who participated in the computer programming and data processing.

Satellite data were furnished by the Photographic Laboratory, Nimbus and ATS Data Utilization Center, Goddard Space Flight Center, NASA.

REFERENCES

Altman, Frederick, J., "Storm Reflectivity Models," Preprints for 14th Radar Meteorology Conference, American Meteorological Society, 1970, pp. 291-295.

BOMAP Office, BOMEX Field Observations and Basic Data Inventory, National Oceanic and Atmospheric Administration, U.S. Department of Commerce, Rockville, Md., 1971, 428 pp.

Borovikov, A.M, V.V. Kostarev, I.P. Mazin, V.I. Smirnov, and A.A. Chernikov, Radar Measurement of Precipitation Rate, Israeli Translation from Russian, U.S. Department of Commerce Clearinghouse for Federal Scientific and Technical Information (now National Technical Information Service), Springfield, Va., 1970, 112 pp.

Center for Experiment Design and Data Analysis (CEDDA), "BOMEX Permanent Archive: Description of Data," NOAA Technical Report EDS 12, National Oceanic and Atmospheric Administration, U.S. Department of Commerce, Washington, D.C., 1975, 327 pp.

Frank, Neil L., "Atlantic Tropical Systems of 1969," Monthly Weather Review, Vol. 98, No. 4, 1970, pp. 307-314.

Hitschfeld, Walter, and Jack Bordan, "Errors Inherent in the Radar Measurement of Rainfall at Attenuating Wavelengths," Journal of Meteorology, Vol. 11, No. 1, 1954, pp. 58-67.

Holland, Joshua Z., "Preliminary Report on the BOMEX Sea-Air Interaction Program," Bulletin of the American Meteorological Society, Vol. 51, No. 9, 1970, pp. 809-820.

Holland, Joshua Z., "The BOMEX Sea-Air Interaction Program: Background and Results to Date," NOAA Technical Memorandum ERL BOMAP-9, Center for Experiment Design and Data Analysis, National Oceanic and Atmospheric Administration, U.S. Department of Commerce, Rockville, Md., 1972a, 34 pp.

Holland, Joshua Z., "Comparative Evaluation of Some BOMEX Measurements of Sea Surface Evaporation, Energy Flux and Stress," Journal of Physical Oceanography, Vol. 2, No. 4, 1972b, pp. 476-486.

Holland, Joshua Z., and Eugene M. Rasmusson, "Measurements of the Atmospheric Mass, Energy, and Momentum Budgets Over a 500-Kilometer Square of Tropical Ocean," Monthly Weather Review, Vol. 101, No. 1, 1973, pp. 45-55.

Holtz, D.C., "A Model of the Distribution of Precipitation in Three Dimensions," Proceedings of the 13th Radar Meteorology Conference, American Meteorological Society, 1968, pp. 110-113.

Hudlow, Michael D., "Weather Radar Investigations on the BOMEX," Research and Development Report ECOM-3320, U.S. Army Electronic Command, Ft. Monmouth, N.J. (Available from Defense Documentation Center or National Technical Information Service), 1970a, 106 pp.

Hudlow, Michael D., "Radar Echo Climatology East of Barbados Derived From Data Collected During BOMEX," Preprints for 14th Radar Meteorology Conference, American Meteorological Society, 1970b, pp. 433-437.

Hudlow, Michael D., "Three-Dimensional Model of Precipitation Echoes for X-Band Radar Data Collected During BOMEX," BOMEX Bulletin No. 10, BOMAP Office, National Oceanic and Atmospheric Administration, U.S. Department of Commerce, Rockville, Md., 1971, pp. 51-63.

Hudlow, Michael D., and Wolfgang D. Scherer, "Precipitation Analysis for BOMEX Period III," NOAA Technical Report EDS 13, Center for Experiment Design and Data Analysis, National Oceanic and Atmospheric Administration, U.S. Department of Commerce, Washington, D.C., 1975, 40 pp.

Huff, F.A., "Spatial Distribution of Heavy Storm Rainfall in Illinois," Water Resources Research, Vol. 4, No. 1, 1968, pp. 47-54.

Jones, R.F., and S.G. Bigler (Chairmen), "Use of Ground-Based Radar in Meteorology," World Meteorological Organization Technical Note No. 78 WMO-No. 193. TP. 99, 1966, pp. 11-13.

Mueller, E.A., and A.L. Sims, "Relationships Between Reflectivity, Attenuation, and Rainfall Rate Derived From Drop-Size Spectra," Final Report (Tech. Rep. ECOM-02071-F), Illinois State Water Survey at the University of Illinois, Urbana, Ill., 1969, 112 pp.

Myers, Vance A., BOMEX Atlas of Satellite Cloud Photographs, BOMAP Office, National Oceanic and Atmospheric Administration, U.S. Department of Commerce, Rockville, Md., 1971, 250 pp.

Probert-Jones, J.R., "The Radar Equation in Meteorology," Quarterly Journal of the Royal Meteorological Society, Vol. 88, No. 378, 1962, pp. 485-495.

Rasmusson, Eugene M., "Mass, Momentum, and Energy Budget Equations for BOMAP Computations," NOAA Technical Memorandum ERL BOMAP-3, BOMAP Office, National Oceanic and Atmospheric Administration, U.S. Department of Commerce, Rockville, Md., 1971, 32 pp.

Sabatini, Romeo R., (Ed.), The Nimbus III User's Guide, Goddard Space Flight Center, National Aeronautics and Space Administration, Greenbelt, Md., 237 pp.

Saunders, Peter M., "Some Characteristics of Tropical Marine Showers," Journal of the Atmospheric Sciences, Vol. 22, No. 2, 1965, pp. 167-175.

Scherer, Wolfgang D., and Michael D. Hudlow, "A Technique for Assessing Probable Distributions of Tropical Precipitation Echo Lengths for X-Band Radar From Nimbus 3 HRIR Data," BOMEX Bulletin No. 10, BOMAP Office, National Oceanic and Atmospheric Administration, U.S. Department of Commerce, Rockville, Md., 1971, pp. 63-68.

Scherer, Wolfgang, D., and Michael D. Hudlow, BOMEX Period III Radar-Satellite Atlas, Center for Experiment Design and Data Analysis, National Oceanic and Atmospheric Administration, U.S. Department of Commerce, Washington, D.C., 1975, 47 pp.

Wilson, James W., "Integration of Radar and Raingage Data for Improved Rainfall Measurement," Journal of Applied Meteorology, Vol. 9, No. 3, 1970a, pp. 489-497.

Wilson, James W., "Operational Measurement of Rainfall With the WSR-57," Final Report CEM 4067-407, The Center for Environment and Man, Inc., Hartford, Conn., 1970b, 44 pp.

Wilson, James W., "Use of Rain Gages To Adjust Radar Estimates of Rainfall," Final Report CEM 4098-448, The Center for Environment and Man, Inc., Hartford, Conn., 1971, 28 pp.

World Meteorological Organization, Commission for Maritime Meteorology (H.U. Roll, Chairman), "Precipitation Measurements at Sea," Technical Note No. 47, WMO-No. 124, TP. 55, Geneva, Switzerland, 1962, 18 pp.

(Continued from inside front cover)

EDS BOMAP-15 Parameterized Moisture and Heat Flux Through Top of BOMEX Volume. Vance A. Myers, May 1975, 8 p. (COM-75-10905/AS)

EDS BOMAP-16 Correction of BOMEX Radiosonde Humidity Errors. L. B. Sanders, J. T. Sullivan, and P. J. Pytlowany, May 1975, 11 p. (COM-75-10992)

EDS BOMAP-17 BOMEX Wind Spectra Derived From the Boundary Layer Instrument Package (BLIP). C. F. Ropelewski, September 1975, 15 p.